frontiers in Earth Science

ORIGINAL RESEARCH
published: 31 March 2022
doi: 10.3389/feart.2022.817682

Two Phases of Metamorphism in the High-Pressure Schists in Central Inner Mongolia, China: Implications for the Tectonic Transition From Terminal Subduction of the Paleo-Asian Ocean to Continental Collision

Jinrui Zhang[1], Shuang Tang[1], Chunjing Wei[2], Hang Chu[3], Wenliang Xu[1] and Ling Jiang[1]*

[1]School of Earth Sciences, Jilin University, Changchun, China, [2]School of Earth and Space Sciences, Peking University, Beijing, China, [3]Tianjin Institute of Geology and Mineral Resources, Tianjin, China

OPEN ACCESS

Edited by:
Yi Chen,
Chinese Academy of Sciences (CAS), China

Reviewed by:
Laixi Tong,
Northwest University, China
Jia Cai,
Chinese Academy of Geological Science, China

****Correspondence:***
Jinrui Zhang
jerryzhang@jlu.edu.cn

Specialty section:
This article was submitted to Petrology, a section of the journal Frontiers in Earth Science

Received: *18 November 2021*
Accepted: *25 February 2022*
Published: *31 March 2022*

Citation:
Zhang J, Tang S, Wei C, Chu H, Xu W and Jiang L (2022) Two Phases of Metamorphism in the High-Pressure Schists in Central Inner Mongolia, China: Implications for the Tectonic Transition From Terminal Subduction of the Paleo-Asian Ocean to Continental Collision. Front. Earth Sci. 10:817682. doi: 10.3389/feart.2022.817682

High-pressure (HP) rocks exhumed from subduction zones usually record much warmer geotherms than numerical modelling results, as their peak mineral assemblages are always modified during the exhumation process. The decompressional metamorphic evolution of HP rocks should be considered carefully if using their P–T records to constrain the thermal structure of a subduction zone. The Ondor Sum Group, known as mélanges containing various high P/T metamorphic rocks in central Inner Mongolia, represents a fragment of subducted oceanic crust in the Early Paleozoic, However, the thermal structure of the subduction zone is unavailable due to an absence of exhumed HP rocks with P–T estimates. In this study, the HP schists were newly discovered in the Ondor Sum Group at Airgin Sum in the central Inner Mongolia. The HP schists include a garnet–phengite schist (sample EL01) and a garnet–amphibole schist (sample EL08). The petrography of these rocks and phase equilibrium modelling using THERMOCALC suggest two phases of metamorphism, both of which are characterized by clockwise P–T evolutions involving pre-peak prograde stage, peak-stage, and post-peak decompression stage. The peak P–T conditions of the early-phase metamorphism are constrained by P–T pseudosections to be ~18 kbar/~535°C for sample EL01 and 18 kbar/~500°C for sample EL08. The peak P–T conditions of the late-phase metamorphism are constrained by P–T pseudosections to be ~8 kbar/532°C in EL01 and ~7.0 kbar/495°C in EL08. Available U–Pb data of zircons from the HP schists and a granodiorite vein using LA–ICP–MS constrain the timing of early-phase HP metamorphism in the early Paleozoic and the late-phase metamorphism supposed to be in the Devonian based on the previous reported ages. The peak P–T conditions for the early-phase metamorphism were high-P/T conditions with a thermal gradient of ~8°C/km, pointing to a warm oceanic subduction. The overprinting late-phase metamorphism represents medium-P/T conditions with a geothermal gradient of 22–25°C/km, which we attribute to a collisional thickening process. As a result, we suggest that the HP schists in the Ondor Sum Group represent the terminal stage of subduction of the Paleo-Asian

oceanic plate, and that the schists were involved in the continental collision after the closure of the Paleo-Asian Ocean in the Devonian.

Keywords: high-pressure schist, ondor sum group, pseudosection, tectonic transition, paleo-asian ocean

1 INTRODUCTION

The thermal structure of subduction zones is controversial as different insights are acquired from geological observations (Tsujimori et al., 2006; Groppo et al., 2009; Penniston–Dorland et al., 2015; Agard et al., 2018; Brown and Johnson, 2018; Holder et al., 2019; Tamblyn et al., 2019) and numerical modelling (e.g., Peacock, 1996; Peacock and Wang, 1999; Syracuse et al., 2010; van Keken et al., 2011; van Keken et al., 2018; van Keken et al., 2019). According to the previous geological studies, metamorphism during oceanic plate subduction is typically of high-P type with geothermal gradients within 5–15°C/km, based mainly on the P–T estimates using traditional methods of high-pressure (HP) rocks exhumed from ancient subduction zones (Miyashiro, 1961, 1994). However, using kinematically defined slabs for obtaining a comprehensive suite of thermal models suitable for the current global subduction system, Syracuse et al. (2010) simulated the thermal structure in 56 segments of active subduction zones. The results suggested that the geothermal gradients along slab surfaces in most oceanic subduction zones range from 3 to 10°C/km, with the P–T conditions mainly located in the metamorphic "forbidden zone" of <5°C/km. Although the numerical modelling results are subject to argument and discussion (Penniston–Dorland et al., 2015; Kohn et al., 2018; van Keken et al., 2018), it is a fact that the HP rocks exhumed from ancient subduction zones generally record much warmer geotherms than numerical modelling results. The mismatch forces us to reevaluate the rigidity and rationality of the P–T estimates for exhumed HP rocks. One uncertainty should be taken into account as the peak mineral assemblages in the exhumed HP rocks are always

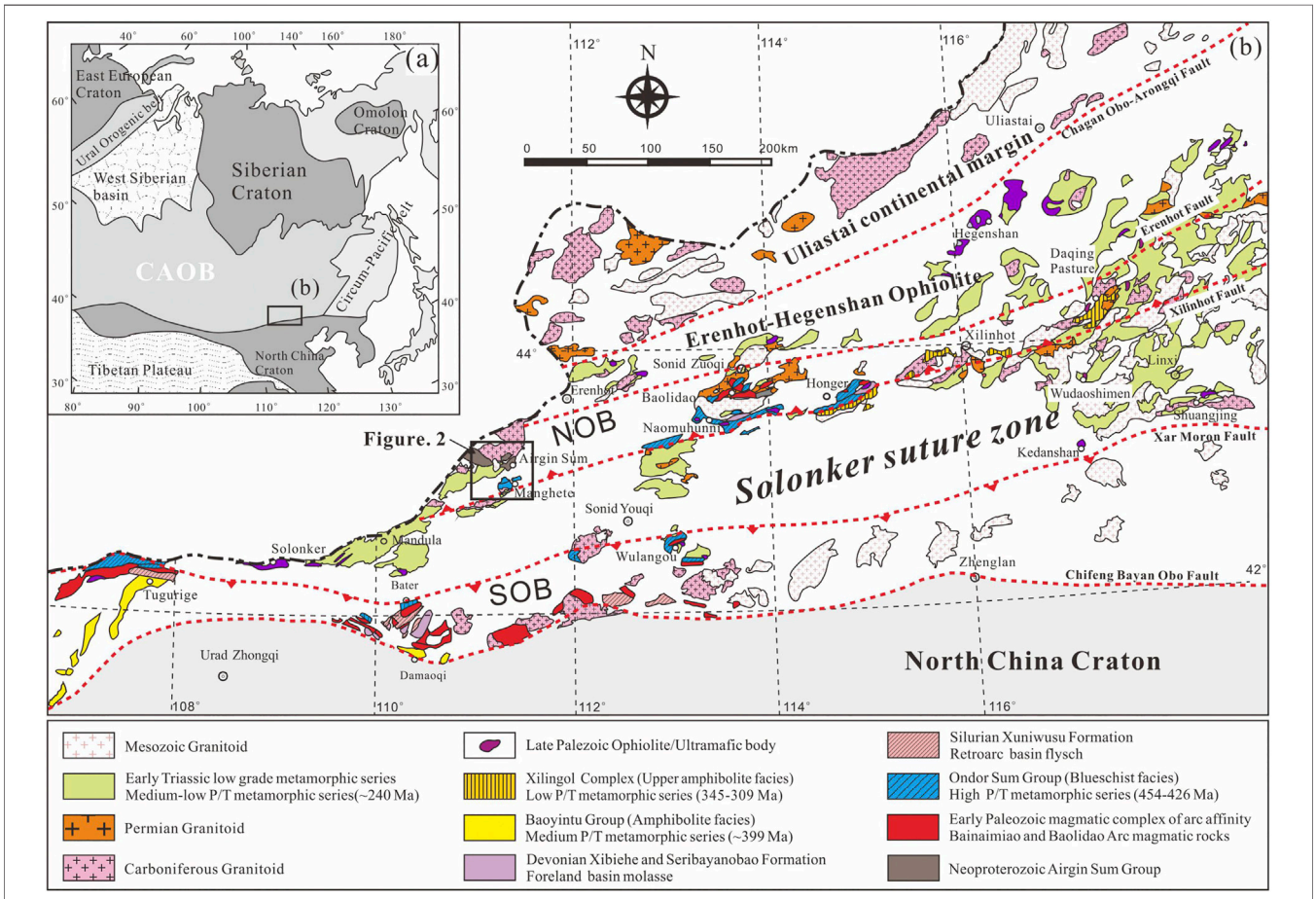

FIGURE 1 | (A) Location of the Central Asian Orogenic Belt (modified after Xu et al., 2013). **(B)** Geological sketch map of the central Inner Mongolia showing the subdivided tectonic units (compiled from IMBGMR, 1991; Jian et al., 2008; Xiao et al., 2003; Xu et al., 2013), and distribution of the Ondor Sum Group.

modified during decompression (Whitney and Davis, 2006; Wei and Clarke, 2011; Tsujimori and Ernst, 2014; Wei and Tian, 2014; Hernánde–Uribe et al., 2018), and this may result in underestimation of the peak pressure or overestimation of the peak temperature related to the metamorphism. Therefore, the decompressional metamorphic evolution of HP rocks should be considered carefully if using their P–T records to constrain thermal structure of a subduction zone.

The early Paleozoic subduction and accretion of the Paleo-Asian oceanic system resulted in various HP metamorphic belts in the Central Asian Orogenic Belt (CAOB) domain. In central Inner Mongolia, the Ondor Sum Group comprises subduction-related mélanges with strongly foliated quartz schists and minor blocks of intermediate–felsic volcanic rocks, pyroclastic tuffs, meta-gabbro, ultramafic rocks, blueschist, chert, and marble (Tang et al., 1983; Tang and Yan, 1993; Xu et al., 2001, 2013; Xiao et al., 2003), which are distributed at Wulangou, Airgin Sum and Naomuhunni (**Figure 1**). At Wulangou, the quartz schists contain high-P/T minerals in an assemblage that includes deerite, glaucophane, lawsonite, phengite, minnesotaite, piemontite, and stilpnomelane (Tang et al., 1983; Tang, 1990). The meta-gabbro also contains sodic amphibole, stilpnomelane, and phengite with a Si content of 3.64 (De Jong et al., 2006). Estimates of the blueschist P–T conditions are 6.0–7.5 kbar/250–300°C, based on the experimental data of Liou et al. (1987) and Maresch (1977) for the stability of lawsonite and glaucophane (Tang and Yan, 1993). At Naomuhunni, an epidote–blueschist block is constrained to be metamorphosed in P–T condition of 6.6–8.1 kbar/420–470°C based on phase equilibria modelling (Xu et al., 2001; Jinrui Zhang et al., 2015). At Airgin Sum, a sodic amphibole-bearing quartzite records P–T conditions of 7–10 kbar/400–450°C (Li et al., 2014) using the garnet–phengite thermometer of Krogh and Råheim (1978). Moreover, a garnet-bearing barroisite schist from the same area records a nearly isothermal decompression from 8.2 to 9.3 kbar/450–500°C to 6–8 kbar/470–500°C, followed by cooling decompression to 2.8 kbar/435°C (Jinrui Zhang et al., 2015). The reported P–T conditions of the above metamorphic rocks indicate medium-P/T facies series rather than the high-P/T facies series. This is attributed to two possibilities: 1) the reported medium-P/T rocks might be the shallower products of subduction other than the exhumed high-P/T products; 2) the absence of peak P–T conditions may be attributed to retrograde metamorphism during uplift or overprinting by tectonic thermal events. Consequently, these reported P-T conditions cannot reveal the thermal structure and evolution of the subduction zone. Moreover, the significance of the corresponding geochronological data needs to be further determined.

In this paper, we report new discoveries of HP schists in the Ondor Sum Group at Airgin Sum in the central Inner Mongolia, including garnet–mica and garnet–amphibole schists. We successfully identify the high-P/T metamorphism and geotherm from the new HP schists using phase equilibria modeling and distinguish it from late decompressional thermal imprint to help construct thermal structure of subduction zones from petrological view. Moreover, based on the zircon U-Pb ages and the previous reported ages, the tectonic significance of the HP schists is also well illustrated.

2 GEOLOGICAL SETTING

The central Inner Mongolia orogenic domain of the Xing' an-Inner Mongolia Orogenic Belt (XIMOB) belongs to the eastern part of the CAOB (**Figure 1**). Multiple tectonic belts/units, including suture zones, accretionary complexes, orogenic belts, and microcontinental blocks have been proposed (e.g., Xiao et al., 2003; Jian et al., 2008, 2010, 2012; Miao et al., 2008; Xu et al., 2013, 2014). However, the schemes of subdivision in terms of the tectonic architecture of this domain remain poorly understood (Xiao et al., 2003; Jian et al., 2008; Xu et al., 2013). In this paper, a preferred alternative scheme is presented based on recent studies of the metamorphism (Zhang et al., 2018b). The major belts include the Southern and Northern Orogenic Belts (SOB and NOB) indicated by Xu et al. (2013), the Solonker suture zone flanked by the SOB and NOB, and the Erenhot–Hegenshan ophiolite belt to the north of the NOB (Xiao et al., 2003), as shown on **Figure 1B**. Their geological characteristics are summarized below.

The SOB consists of subduction-related mélanges, magmatic complexes of arc-affinity, sedimentary sequences of retro-arc and foreland basins, and various metamorphic rocks. The mélanges are known as the Ondor Sum Group, and it has been suggested to be metamorphosed during subduction at 454–426 Ma ($^{40}Ar/^{39}Ar$ ages) (Tang and Yan, 1993; De Jong et al., 2006). The magmatic complex of arc-affinity includes a volcanic sequence of basic to acidic rocks (499–440 Ma) known as the Bainaimiao Group (Zhang et al., 2010), as well as plutons of diorite, gabbro, and granitoid with ages of 490–425 Ma (Liu et al., 2003; Jian et al., 2008; Xu et al., 2013). The sedimentary sequences comprise the Silurian flysch of the Xuniwusu Formation and the Lower Devonian molasse of the Xibiehe Formation, which are respectively interpreted to represent deposition in retro-arc and foreland basins (Xu et al., 2013). The medium-P/T metamorphic rocks located in the west Tugurige area are grouped together as the Baoyintu Group, and it has been proposed recently that they are the products of a collisional process at ca. 399 Ma (Chen et al., 2015). These units in the SOB have been interpreted in terms of a tectonic evolution during the early Paleozoic from southward subduction of the Paleo-Asian oceanic plate to subsequent collision (Jian et al., 2008; Xu et al., 2013; Chen et al., 2015).

The NOB has similar configuration to the SOB. The mélanges are also known as the Ondor Sum Group, and a blueschist block at Naomuhunni yielded a glaucophane $^{40}Ar/^{39}Ar$ age of 383 ± 13 Ma (Xu et al., 2001). The magmatic complexes with arc affinities are distributed from Baolidao through Xilinhot to Daqing Pasture, and they consist of cumulate gabbros, gabbro-diorites, quartz diorites, tonalites, and granites with ages of 482–428 Ma (Chen et al., 2000; Shi et al., 2004, 2005; Jian et al., 2008; Xue et al., 2009). The foreland molasse sequences are grouped together as the Devonian Seribayanobao Formation, and they unconformably overlie the mélanges (Xu et al., 2013).

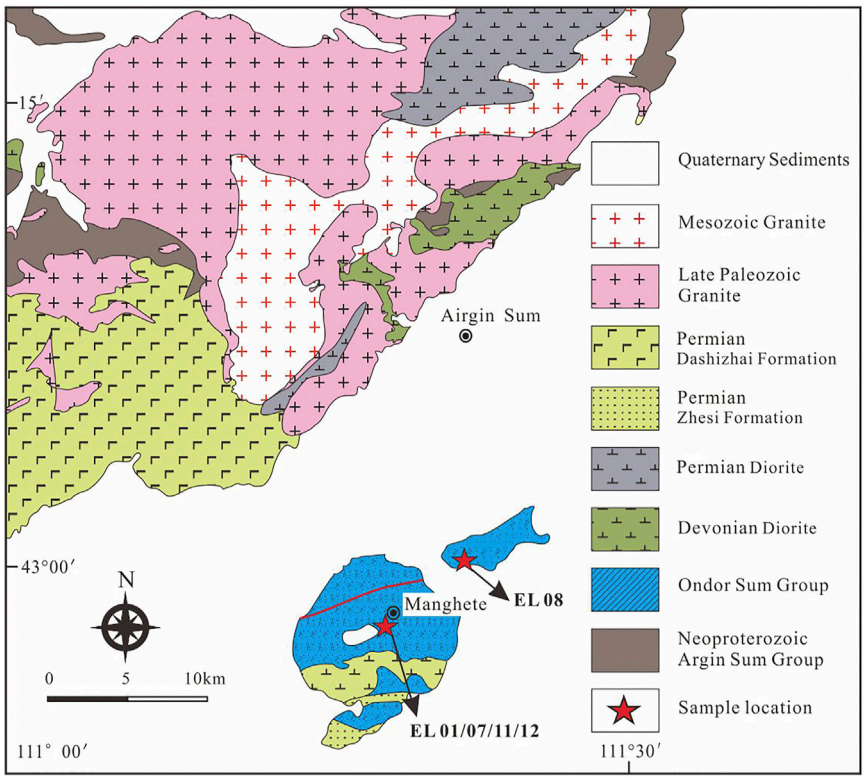

FIGURE 2 | Geological map of Airgin Sum area (modified after Li et al., 2014) showing lithological distribution of the Ondor Sum Group and sampling localities.

The Xilingol Complex of metamorphic rocks underwent HT–LP metamorphism at 345–309 Ma in relation to the extensional processes of a previous orogeny (Zhang et al., 2018b). It has been suggested that these tectonic units represent a northward subduction–collision system in central Inner Mongolia (Xu et al., 2013). Precambrian terranes in the area include the Airgin Sum Group, which is composed mainly of low-grade mica-schists and metasandstones with an upper intercept age of 952 ± 8 Ma (IMBGMR, 1991) and an age peak at 1,180 Ma (Xu et al., 2014), as well as 1,516 ± 31 Ma gneissic granites at Sunidzuoqi (Sun et al., 2013), and together these Precambrian rocks are classified as part of the Southern Mongolian Block (Badarch et al., 2002; Yarmolyuk et al., 2005, 2008; Xu et al., 2014).

The Solonker suture zone and the Erenhot–Hegenshan ophiolite belt are both marked by sporadic distributions of various ophiolitic fragments such as metabasalts, serpentinized harzburgites, dunites, and gabbroic cumulates. The suture zone has an age of 297–250 Ma (Xiao et al., 2003; Miao et al., 2008; Jian et al., 2010, 2012) and the Erenhot–Hegenshan ophiolite belt an age of 354–300 Ma (Liu et al., 2012; Zhang et al., 2014; Song et al., 2015; Zhicheng Zhang et al., 2015). They were once considered evidence of the continuous evolution of the Paleo-Asian oceanic system during the late Paleozoic (Xiao et al., 2003). However, more recent studies have indicated that the basic rocks exhibit characteristics of N-MORB and E-MORB, or supra-subduction zone-type oceanic crust that might have formed in back-arc basins (Song et al., 2015) or limited ocean basins (Chu et al., 2013; Jinrui Zhang et al., 2015; Wang et al., 2015).

The tectonic belts mentioned above were extensively intruded by the late Paleozoic granitic plutons including the Carboniferous and Permian granitoids (**Figure 1B**). However, these plutons are still variously and controversially interpreted as the products of subduction (Zhang et al., 2007, 2009; Liu et al., 2009) or post-orogenic extension (Shi et al., 2003; Zhang et al., 2014; Tong et al., 2015; Qiao et al., 2017). Recent research has revealed that the widely distributed Carboniferous–Permian volcanic and sedimentary sequences along the Solonker suture zone were metamorphosed to greenschist and local amphibolite facies low–medium-P series rocks in the Early Triassic (~240 Ma), and it was suggested that this metamorphism resulted from the closure of limited ocean basins (Chen et al., 2012; Zhang et al., 2016). Moreover, it has been suggested that the 222–204 Ma monzogranites and syenogranites at Xilinhot and Sunidzuoqi (Liu et al., 2005) and the 238–204 Ma peraluminous granites at Shuangjing formed in a setting of crustal thickening (Li et al., 2007).

The Ondor Sum Group is characterized by typical configurations containing various blocks and heterogeneously deformed matrix (Xu et al., 2013). The matrix consists mainly of interbedded sericite–quartz schist, chlorite–quartz schist, and mica-schist, and the blocks include quartzite (sodic-amphibole-bearing locally), ultramafic rocks,

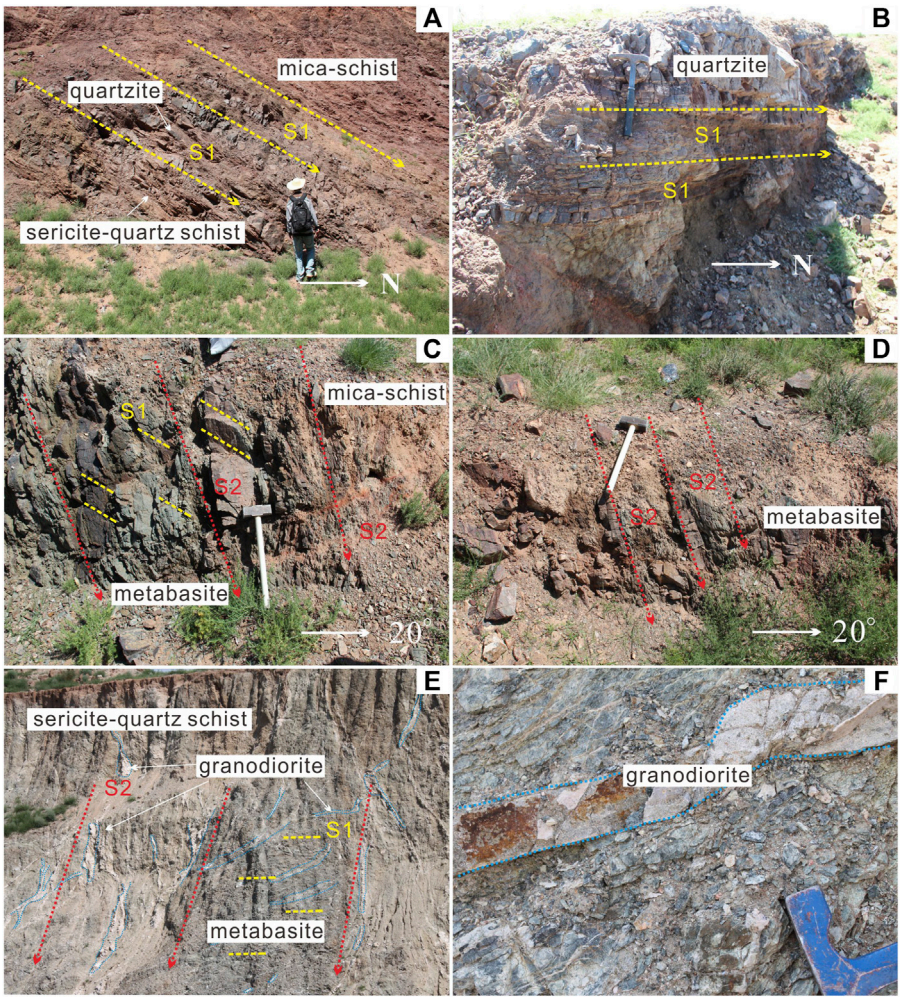

FIGURE 3 | Field photographs showing rocks of different types in the Ondor Sum Group at Airgin Sum, including quartzite **(A,B)**, sericite-quartz schist **(A)**, mica-schist **(A,C)** and metabasite **(C,D)**, and granodiorite veins **(E,F)**. Two phases of foliations (S1 and S2) are observed in the outcrops.

limestone, and metabasite as well as barroisite schist. Along with the Ondor Sum Group also distributes the Airgin Sum Group, Permian volcanic and sedimentary sequences such as the Dashizhai and Zhesi formations, and late Paleozoic and Mesozoic plutons (**Figure 2**). In the field of Airgin Sum, the matrix is composed dominantly of sericite–quartz schist, intercalated with minor amounts of garnet mica-schist (HP rocks in this study) that runs in strips parallel to the foliation of the sericite–quartz schist. Several blocks within the matrix are quartzites and metabasites, found mostly through exploratory drilling. The quartzites had already been reported by Li et al. (2014) to locally contain sodic-amphibole. The metabasites are garnet amphibole schists (HP rocks in this study) along with minor greenschist. Multiphase deformations have been recorded in the Ondor Sum Group, including the early S1 foliation that dips mainly to the north in the quartzite, mica-schist, sericite–quartz schist, and metabasite outcrops (Xu et al., 2013; **Figures 3A–C**), and the nearly-vertical late S2 foliation that displaces the early S1 foliation (Xu et al., 2013; **Figures 3D,E**). Moreover, the HP schists are intruded by granodiorite veins locally. These veins are observed to be striking parallel to S1 foliation initially but modified later by S2 foliation, indicating that the granodiorite veins were formed later than S1 but earlier than S2 (**Figure 3F**).

Samples for this study were collected from the Ondor Sum group in Manghete, ~20 km south of the Airgin Sum area (**Figure 2**). They include different HP schist samples such as two garnet–mica schist samples (EL01 and EL07), a garnet–amphibole schist sample (EL08) and a sericite–quartz schist sample (EL11) intercalated with the garnet-mica schist. Moreover, a granodiorite sample (EL12) intruding in the HP schist was also selected. It should be noted that the HP samples EL01 and EL08 are for petrological analyses and phase equilibria modeling as these two samples are observed to preserve multistage mineral assemblages and deformations which are available to better reveal the metamorphic evolution. Other samples are only for zircon U-Pb dating.

TABLE 1 | Bulk-rock compositions of the HP schists at Airgin Sum.

ICP–OES whole rock compositions (wt%)															
Sample	**SiO_2**	**TiO_2**	**Al_2O_3**	**$Fe_2O_3^T$**	**FeO**	**MnO**	**MgO**	**CaO**	**Na_2O**	**K_2O**	**P_2O_5**	**LOT**	**Total**	**$Mg^{\#}$**	**A/CNK**
EL01	69.86	0.79	12.57	5.66	0.00	0.28	2.73	1.10	1.43	2.57	0.21	2.99	100.19	0.49	1.76
EL08	48.52	1.76	13.48	12.72	0.00	0.20	6.50	10.43	2.63	0.21	0.22	3.63	100.30	0.51	
Normalized molar proportion used for phase equilibria modeling (mole%)															
Sample	**Figs**	**SiO_2**	**Al_2O_3**	**CaO**	**MgO**	**FeO**	**K_2O**	**Na_2O**	**TiO_2**	**MnO**	**O**				
EL01	**Figures 6,7**	77.33	8.20	0.98	4.50	4.71	1.81	1.53	0.66	0.26	0.10				
EL08	**Figures 8,9**	53.46	8.75	10.63	10.68	10.55	0.14	2.81	1.46	0.19	2.33				

LOI, loss on ignition; $Fe_2O_3^T$: total Fe_2O_3 in ICP–OES, analyses; $Mg^{\#}$ = MgO/(MgO + FeO) in mole.
A/CNK, $Al_2O_3/(^{CaO}$ + Na_2O+ K_2O) in mole.

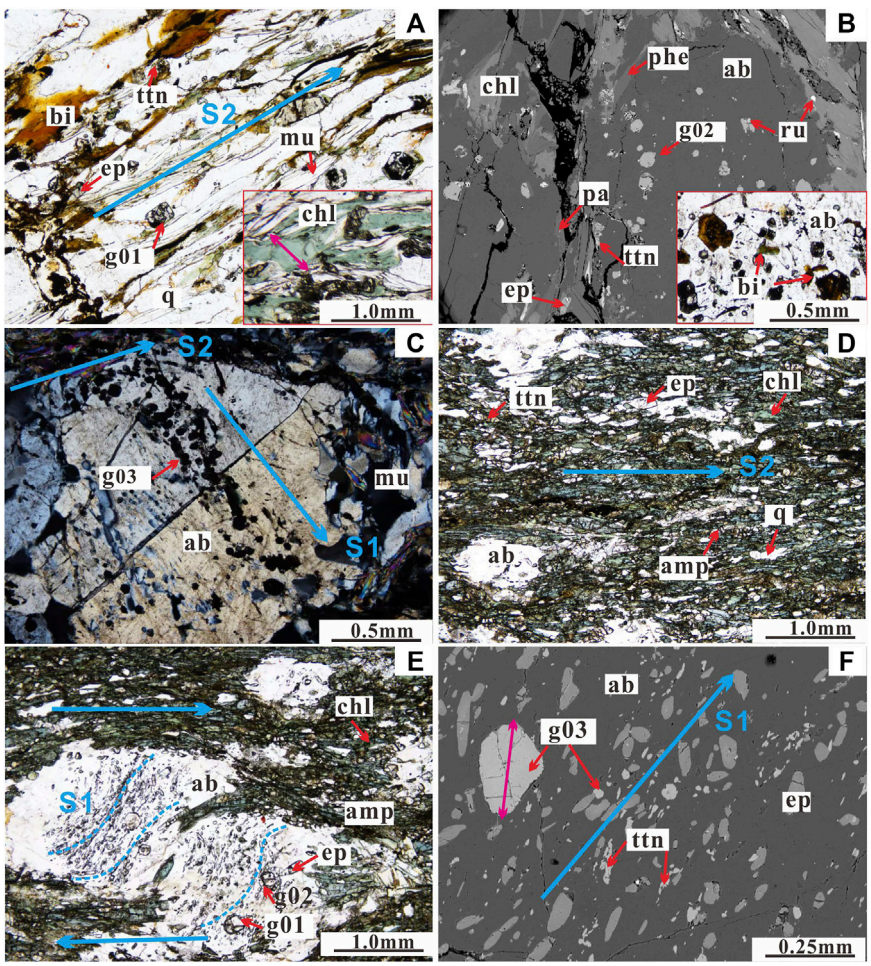

FIGURE 4 | Microphotographs of newly discovered schists from the Ondor Sum Group at Airgin Sum, central Inner Mongolia. **(A)** The foliated matrix composed of phengite, biotite, epidote, chlorite and titanite (S2 foliation) in sample EL01; **(B)** The BSE images showing albite porphyroblasts enclosing the early fine-grained garnet and the matrix minerals such as phengite, paragonite, biotite, quartz and rutile as inclusions; **(C)** The oriented garnet inclutions in albite porphyroblasts showing the early foliation (S1) in sample EL04; **(D)** The foliated matrix composed of amphibole, albite, chlorite, epidote and titanite (S2 foliation) in sample EL08; **(E)** The syntectonic albite porphyroblast showing dextral movement along foliation S2 with oriented inclusions (S1) in sample EL08; **(F)** The BSE images showing inclusions of albite porphyroblast such as garnet, epidote, amphibole and titanite in sample EL08. The measured garnet grains are shown with double sided arrow. Mineral abbreviations: bi, biotite; mu, muscovite; ep, epidote; chl, chlorite; amph, amphibole; g, garnet; phe, phengite; ab, albite; q, quartz; ttn, titanite; ru, rutile; pa, paragonite; q, quartz.

3 PETROLOGICAL ANALYSES

3.1 Analytical Methods

The bulk-rock compositions of samples EL01 and EL08 were determined by a Leeman Prodigy inductively coupled plasma optical emission spectrometer (ICP–OES) system with high dispersion Echelle optics at China University of Geoscience (Beijing). Standard basalt GSR3 was used for calibration. The loss on ignition was determined routinely and the relative analytical uncertainties for all elements are <3%. The results are presented in **Table 1**. Mineral microprobe analyses were carried out at the Key Laboratory of Orogenic Belts and Crustal Evolution of Peking University. The minerals were analyzed using a JXA-8100 electron microprobe in wavelength-dispersive mode with 15 kV acceleration potential, 15 nA beam current, and a counting time of 20–30 s. The beam diameter was set to 1 μm for all phases except for muscovite, which was analyzed using a 5 μm beam diameter. Natural and synthetic minerals were used for standardization. Relative analytical uncertainties are <2% for major elements. The analyses of samples EL01 and EL08 are presented in **Supplementary Appendixs S1, S2**. Photomicrographs of the two samples are shown in **Figure 4**.

3.2 Bulk-Rock Compositions

The garnet–mica schist EL01 has content of SiO_2 = 69.86 wt%, Na_2O = 1.43 wt%, K_2O = 2.57 wt%, CaO = 1.10 wt%, A/CNK = 1.76, and $Mg^{\#}$ = 0.49, which is likely to represent an aluminum-rich graywacke or volcanic sedimentary rock from an ocean trench (Li et al., 2014). The garnet–amphibole schist EL08 is a typical basic rock with contents of SiO_2 = 48.52 wt%, Al_2O_3 = 13.48 wt%, $Fe_2O_3^T$ = 12.72 wt%, MgO = 6.50 wt%, CaO = 10.43 wt%, and Na_2O = 2.63 wt%, with an $Mg^{\#}$ value of 0.51 (Zhang et al., 2014).

3.3 Petrography and Mineral Compositions

Sample EL01 contains garnet (5 vol%), white mica (30 vol%, muscovite and phengite), biotite (10 vol%), albite (16 vol%), quartz (28 vol%), and chlorite (6 vol%) along with minor paragonite (2 vol%), epidote (2 vol%), and accessory titanite, and rutile (**Figure 4A**). Albite occurs as porphyroblasts that are 2–3 mm across (**Figure 4B**) that grew over a fine-grained and well foliated matrix defined by oriented muscovite, biotite, quartz, and chlorite (S2, **Figure 4A**). A few albite porphyroblasts contain numerous inclusions of garnet, phengite, biotite, paragonite, and rutile that are oriented to form an early-phase foliation (S1 in **Figures 4B,C**). The albites commonly have low values of X_{An} (0.01–0.03) in cores and mantles, but high values of X_{An} (0.06) in the rims. Garnet occurs as inclusions in albite and as subhedral to euhedral grains of 0.05–0.20 mm in the matrix, and they exhibit different compositions in these two places. A measured garnet in the matrix (g01) exhibits asymmetric zoning. The right half of **Figure 5A** shows increasing almandine from core to rim (0.41→0.58, = $Fe^{2+}/(Fe^{2+}$ + Mg + Ca + Mn), others are defined accordingly), increasing pyrope (0.06→0.07), but decreasing spessartine (0.33→0.19) and grossular (0.20→0.16). The left half of **Figure 5A** shows a similar core-to-mantle trend as the right half but is rimmed by a precipitous increase of grossular (0.23–0.28) and decrease of spessartine (0.10–0.06), coupled with pyrope (0.08–0.10) and almandine (0.56–0.57). Two measured garnet grains (g02 and g03) from within an albite porphyroblast show increasing grossular from cores to rims (0.14→0.27 in g02 and 0.17→0.29 in g03) coupled with decreasing spessartine (0.17→0.09 in g02 and 0.16→0.06 in g03). Their almandine

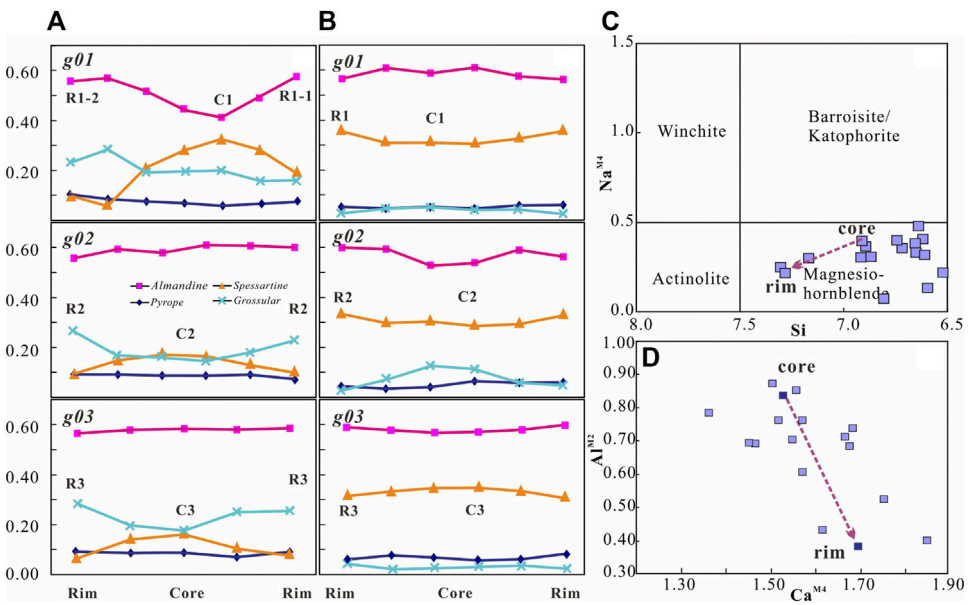

FIGURE 5 | The zoning profiles of almandine, pyrope, grossular and spessartine for the representative garnet grains in sample EL01 **(A)** and sample EL08 **(B)**, and the Si *vs*. Na^{M4} p. f.u. **(C)** and Ca^{M4} *vs*. Al^{M2} **(D)** diagram showing the compositions of amphibole in the sample EL08 (after Leake et al., 1997).

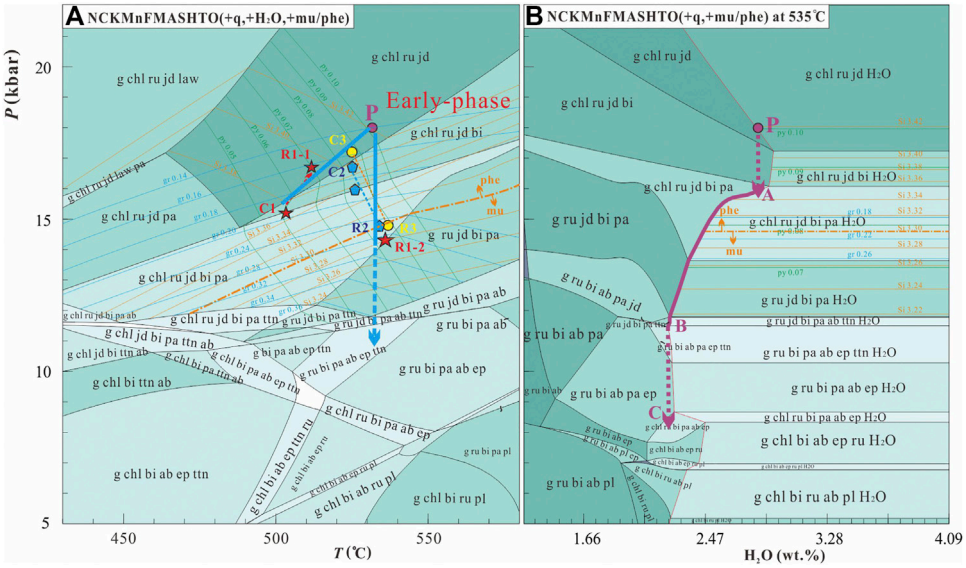

FIGURE 6 | (A) *P–T* pseudosection for sample EL01 calculated in the system NCKMnFMASHTO (+q, H_2O, mu/phe) using the modified bulk-rock composition from Table 1, and **(B)** P-M(H_2O) pseudosection calculated at temperature of 535°C. The pseudosections show isopleths of *py* (pyrope) and *gr* (grossular) in garnet and Si content in phengite for relevant mineral assemblages. The plots of the measured pyrope and grossular in the core and rim of different garnet grains (g01, g02, and g03) are shown as different shapes marked with C (C1, C2, and C3) and R (R1, R2, and R3). The R1-1 and R1-2 represent right and left rim of the grain g01. Mineral abbreviations: law, lawsonite; ctd, chloritoid; o, omphacite; jd, jadeite, pl, plagioclase others are the same as in **Figure 3**.

(0.55–0.61 in g02 and 0.56–0.59 in g03) and pyrope (0.07–0.09 in g02 and 0.07–0.09 in g03) contents are nearly constant, although some analyses show slight fluctuations (**Figure 5A**). Biotite in the matrix and as inclusions are both found altered to chlorite with X_{Mg} values of 0.54–0.61 and small amounts of K = 0.37–0.52 p.f.u. (per formulae unit). Phengite generally occurs as inclusions in the albite and has Si = 3.31–3.42 p.f.u. and Mg = 0.26–0.34 p.f.u., while muscovite in the matrix has lower values of Si = 3.19–3.26 p.f.u. and Mg = 0.23–0.24 p.f.u. Paragonite flakes mostly intergrown with phengite have Na = 0.82–0.93 p.f.u. Chlorite forms either large porphyroblasts 1–2 mm across or micro-flakes in the matrix. Most have X_{Mg} values [= Mg/(Fe^{2+} + Mg)] of 0.58–0.66. A measured chlorite flake shows an increase in X_{Mg} from core to rim of 0.59–0.64. Epidote has pistacite contents (Ps = Fe^{3+}/(Fe^{3+} + Al)) of 0.15–0.19. According to the above observations, two phases of mineral assemblage can be inferred: an early phase that is characterized by the coexistence of garnet and phengite together with paragonite, biotite, and rutile as inclusions, and a late phase that is marked by the formation of albite porphyroblasts together with muscovite, biotite, chlorite, epidote, and titanite. Moreover, we suggest that these two phases of mineral assemblage correspond to the two phases of foliations.

Sample EL08 contains amphibole (37 vol%), albite (20 vol%), garnet (4 vol%), epidote (16 vol%), chlorite (8 vol%), and quartz (12 vol%) together with minor titanite (**Figure 4D**). Albite occurs as porphyroblasts 1–3 mm across that grew over a well-foliated matrix defined by oriented amphibole, titanite, epidote, and chlorite (S2, **Figure 4E**). The albite porphyroblasts locally developed pressure shadows that indicate dextral shearing (**Figure 4E**). The albites have X_{An} < 0.05 and contain numerous inclusions of garnet, epidote, titanite, and quartz that are oriented, forming an early-phase foliation (S1 in **Figure 4F**). The S1 foliation commonly displays S-shapes: the part that is in the core domain of an albite shows a uniform orientation, but this is gradually deflected outside the core to be consistent with S2 near the rim, indicating a syntectonic origin for the albite. The amphiboles are deep to light blue–green and form prismatic crystals in the matrix and inclusions in the outer rims of the albite porphyroblasts (**Figure 4E**). Two occurrences of amphibole show magnesio-hornblende compositions (Leake et al., 1997) with Si = 7.30–6.44 p.f.u., Al^{M2} = 0.87–0.38 p.f.u., Na^{M4} = 0.49–0.08 p.f.u., and Ca^{M4} = 1.75–1.36 p.f.u. (**Figures 5C,D**). Moreover, one measured amphibole grain exhibits zoning with Al^{M2} decreasing from 0.85 p.f.u. to 0.43 p.f.u. from core to rim and Na^{M4} decreasing from 0.37 p.f.u. to 0.25 p.f.u. Garnets only occur as 0.05–0.2 mm inclusions within the albite porphyroblasts. Three analyzed grains display increasing pyrope from core to rim (0.04→0.06 in g01 and g02, 0.05→0.08 in g03), coupled with fluctuations in grossular (0.31→0.36 in g01, 0.30→0.29 in g02, and 0.35→0.33 in g03), spessartine (0.04→0.02 in g01, 0.13→0.06 in g02, and ~0.02 in g03), and almandine (0.61→0.56 in g01, 0.53–0.59 in g02, and 0.57→0.58 in g03, **Figure 5B**). Epidote is present in the matrix and as inclusions within the albite porphyroblasts, and they all have similar compositions with Ps (Fe^{3+}/(Fe^{3+} + Al)) = 0.16–0.24. Chlorite also occurs both in the matrix and as inclusions in the albite, and its values of X_{Mg} (Mg/(Fe^{2+} + Mg)) = 0.59–0.60. The above observations suggest two phases of mineral assemblage: an early phase represented by the garnet-bearing inclusions within

albite, and a late phase marked by the formation of albite porphyroblasts together with the matrix minerals, and these two phases of mineral assemblage also correspond to the two phases of foliation development.

4 PHASE EQUILIBRIA MODELLING AND P–T CONDITIONS

Phase equilibria were modeled for samples EL01 and EL08 in the system NCKMnFMASHTO (Na_2O–CaO–K_2O–MnO–FeO_{total}–MgO–Al_2O_3–SiO_2–H_2O–TiO_2–Fe_2O_3). This system provides a realistic compositional approximation of the studied rocks, within which the early-phase assemblages with garnet can be calculated. The pseudosection modelling was done for the garnet–phengite schist EL01 and the garnet–amphibole schist EL08 using THERMOCALC 3.45 with the internally consistent thermodynamic dataset (ds62) of Holland and Powell (2011). The mixing models were those presented for clinopyroxene and amphibole (Green et al., 2016), garnet, orthopyroxene, and biotite (White et al., 2014), plagioclase (Holland and Powell, 2003), muscovite (Coggon and Holland, 2002), chlorite (Holland and Powell, 1998), ilmenite (White et al., 2000), and epidote (Holland and Powell, 1998). Rutile, titanite, and paragonite are pure end-member phases. Quartz and the fluid phase (assumed to be pure H_2O) were in excess.

For the modelling of the early-phase assemblages of sample EL08, the bulk-rock compositions given by the ICP–OES analyses were used, normalized to mole proportions according to the model system. The O (Fe_2O_3) values were estimated on the basis of mass balance constraints by adding up the Fe^{3+} contents of each mineral (**Table 1**). However, in sample EL01, the chloritization of biotite resulted in a loss of a certain amount of K_2O from the bulk-rock compositions given by ICP–OES analyses, which therefore may not be appropriate for modelling the early phase metamorphism. Thus, an effective bulk composition was generated for sample EL01 following the method of Carson et al. (1999) by integrating mineral compositions (using a standard biotite composition with X_{Mg} = 0.60 after Li et al., 2014) and modal abundance data for the phases present. The bulk-rock compositions for the calculated pseudosections are listed in **Table 1**.

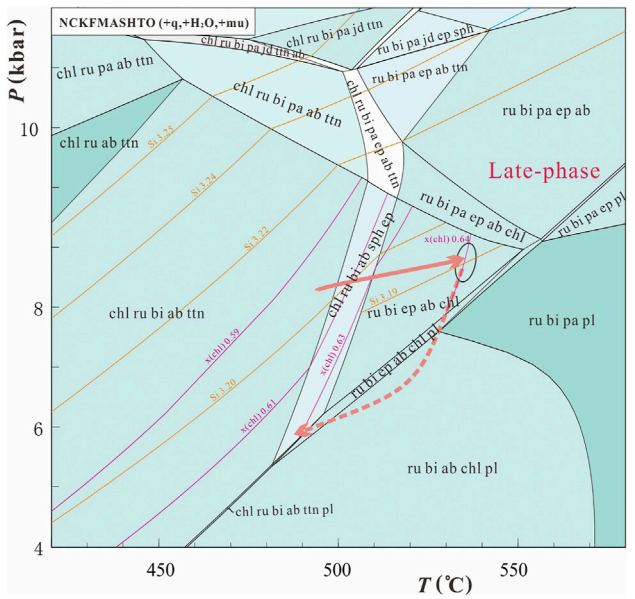

FIGURE 7 | *P–T* pseudosection for sample EL01 calculated in the NCKFMASHTO (+q, H_2O, mu) using an effective bulk composition generated according to mass balance constraints by excluding the composition of garnet and integrating mineral compositions and modal abundance data of the other phases, normalized on the basis of mole-proportions as: SiO_2 = 79.44, Al_2O_3 = 7.95, CaO = 0.52, MgO = 4.57, FeO = 3.60, K_2O = 1.93, Na_2O = 1.63, TiO_2 = 0.68, and O = 0.09 (mol%). The pseudosections show isopleths of Si content in muscovite and x (chl) { = $Mg/(Fe^{2+} + Mg)$} for relevant mineral assemblages.

4.1 Pseudosections for Sample EL01

The P–T pseudosection calculated for sample EL01 in the NCKMnFMASHTO system is presented in **Figure 6A**. The albite-absent assemblages occur at higher pressures above 10–13 kbar, and the titanite-present assemblages occur in the lower P–T range of <8–12 kbar/500°C. The inferred early-phase assemblage of garnet, phengite, paragonite, biotite, and rutile without albite cannot match any predicted assemblage in the pseudosection. However, the pyrope and grossular compositions of the garnet constrain P–T conditions in jadeite-bearing assemblages. The matrix-garnet defined prograde P–T vector from ~15 kbar/~503°C to ~17 kbar/~515°C (C1→R1-1) is based on the core-to-rim zoning shown in the right part of **Figure 5A**, and the retrograde P–T condition of ~14 kbar/~540°C (R1-2) is based on the rim in the left part of the diagram. Moreover, the core–rim zoning of two garnet grains included within albite defines a dominantly decompressional P–T path from ~16 to ~14 kbar at a temperature of ~530°C (C2→R2 and C3→R3). The plotting of the measured Si = 3.34–3.31 p.f.u in phengite is roughly consistent with the P–T conditions defined by the garnet cores. However, the measured Si = 3.42–3.38 p.f.u in phengite indicates a higher pressure that is more likely to represent the peak condition. This peak P–T condition can be constrained to ~18 kbar/~535°C, based on the maximum Si content in phengite and pyrope in garnet, while the grossular content of the garnet was likely modified during the decompressional stages.

To illustrate the post-peak decompressional metamorphic evolution, a P–M (H_2O) pseudosection was calculated at T = 535°C (**Figure 6B**), which shows that the predicted peak assemblage contains 2.82 wt% H_2O. The decompressional path from the inferred peak condition (P) deviates from the H_2O-saturated curve, and proceeds in H_2O-absent conditions. At ~16 kbar (A), the path returns to H_2O-saturated conditions and evolves along the H_2O-saturation line to lower M (H_2O), and with successive dehydration the modes of paragonite and biotite growth increase together with decreasing modes of jadeite, chlorite, and phengite. The final disappearance of jadeite

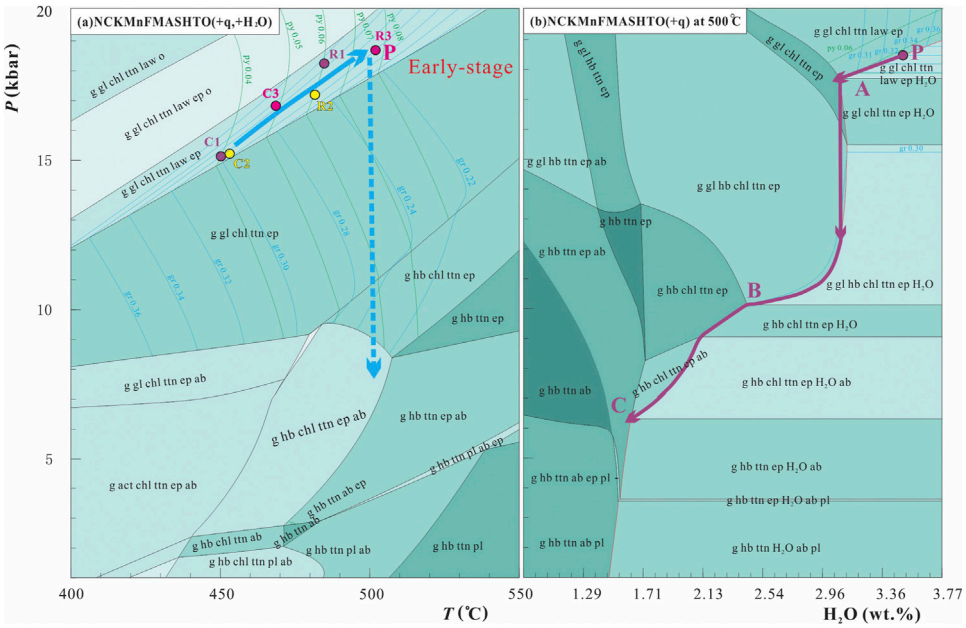

FIGURE 8 | (A) *P–T* pseudosection for sample EL08 calculated in the system NCKMnFMASHTO (+q, H_2O) using the modified bulk-rock composition from **Table 1** and **(B)** P–M (H_2O) pseudosection calculated at temperature of 500°C. The pseudosection is contoured with isopleths of pyrope (py) and grossular (gr) in garnet. The plots of the measured pyrope and grossular in the core and rim of different garnet grains (g01, g02, and g03) are shown as different shapes marked with C (C1, C2, and C3). It is noted that the subtypes of amphibole used in pseudosections follow those in Diener et al. (2007) where glaucophane (gl) refers to sodic amphibole, actinolite (act) refers to calcic amphibole and hornblende (hb) refers to sodic-calcic amphibole or calcic amphibole. Others are the same as in **Figures 4**, **7**.

occurs in a narrow pressure range with the presence of both jadeite and epidote at ~11.8 kbar (B), accompanied by a pronounced release of water with H_2O down to ~2.23 wt%. As further decompression may occur under fluid-absent conditions if there is no infiltration of water to saturate the rock, the mineral assemblage (g + chl + pa + bi + ru + ep) at this point tends to be preserved (Guiraud et al., 2001; Wei and Clarke, 2011). In this case, the metamorphic evolution may continue with the formation of a late-phase mineral assemblage represented by the S2 foliation and especially the growth of albite porphyroblasts, which possibly represent the overprinting of a separate metamorphic–deformational event.

The inferred late-phase assemblage that is marked by the presence of albite porphyroblasts together with chlorite, epidote, and titanite is predicted to stabilize under P–T conditions of <10 kbar and <520°C (**Figure 6A**). However, this prediction may not be valid, because the post-peak metamorphic evolution would have been controlled by local equilibrium domains as a result of the widespread preservation of early-phase minerals. To investigate the metamorphic evolution of the late-phase assemblage, an alternative P–T pseudosection was calculated in the system NCKFMASHTO, using an effective bulk composition that was generated following Carson et al. (1999) by excluding the components frozen in the early-phase assemblage. As shown in **Figure 7**, the inferred late-phase assemblage that includes muscovite, biotite, epidote, chlorite, and rutile is predicted to stabilize in the P–T range of 5–9 kbar/500–550°C. The isopleths of the measured Si = 3.19 in muscovite and x (chl) = 0.64 in chlorite can yield a P–T condition of ~8 kbar/532°C, which is in good agreement with that defined from the inferred assemblage. Under this condition, the rock may contain 2.69–3.05 wt% H_2O, which is a much higher value than when jadeite disappears (~2.23 wt%), and this indicates that infiltration of water occurred during the late-phase metamorphic evolution. Moreover, the core–rim increase in chlorite X_{Mg} from 0.59 to 0.64 predicts a prograde metamorphic evolution characterized by increasing temperature, and the measured rims of albite with higher X_{An} probably indicate decompression to the plagioclase-stable assemblage.

4.2 Pseudosections for Sample EL08

The *P–T* pseudosection for sample EL08 is presented in **Figure 8A**. The inferred early-phase garnet-bearing and albite-absent assemblages can occur at high pressures above 8–10 kbar. The contours of the measured core–rim zoning in garnet grains yield a prograde *P–T* vector from 15 kbar/~450°C to 18 kbar/~500°C (C1→R1 for g01, C2→R2 for g02, and C3→R3 for g03 in **Figure 5B**) in the assemblage with lawsonite and glaucophane, neither of which have been observed in the rock. If it is assumed the post-peak decompression was isothermal, the metamorphic evolution can be documented in the P–M (H_2O) pseudosection at 500°C (**Figure 8B**). The decompressional path from the peak condition (P) may evolve along the H_2O-saturation line to lower M (H_2O), characterized by lawsonite decomposition through successive dehydration reactions, and releasing a large amount of H_2O (3.52→3.10 wt%). On the disappearance of lawsonite at

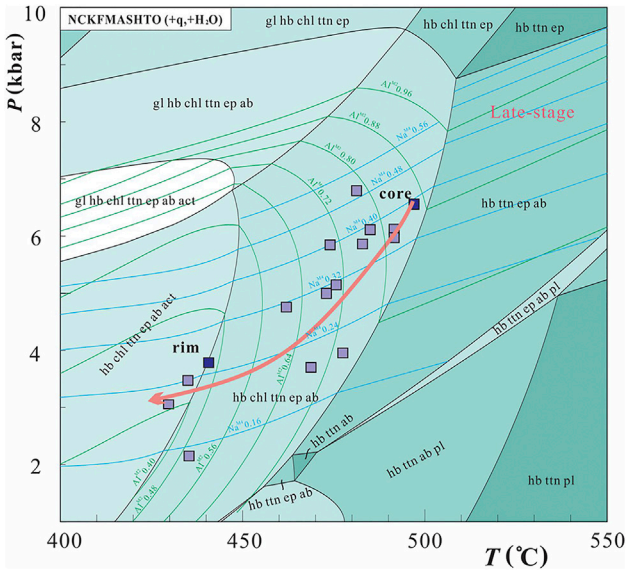

FIGURE 9 | *P–T* pseudosection for sample EL08 calculated in the NCKFMASHTO (+q, H_2O) using an effective bulk composition generated by the same method as in **Figure 7**, normalized on the basis of mole-proportions as: SiO_2 = 54.07, Al_2O_3 = 8.60, CaO = 10.47, MgO = 10.92, FeO = 9.98, K_2O = 0.15, Na_2O = 2.92, TiO_2 = 1.52, and O = 2.40 (mol%). The pseudosection is contoured with isopleths of Al^{M2} and Na^{M4} in calcic-amphibole. Plots of cacic-amphibole compositions are shown as squares and labels C and R correspond to those in **Figure 5**.

~17.5 kbar (A), the decompressional path may deviate from the H_2O-saturated curve and proceed under H_2O-absent conditions. At ~12 kbar (B), the path will return to H_2O-saturated conditions. Further decompression would see equilibria evolving along the H_2O-saturation line to lower M (H_2O), resulting in glaucophane giving way to hornblendic amphibole (C). Thus, a prediction of the decompressional path P→C is that both lawsonite- and glaucophane-bearing assemblages are unlikely to be preserved due to a series of dehydration reactions, and the inclusions in albite are more likely to be g + hb + chl + ttn + ep than other higher pressure phases. A further notable dehydration reaction is predicted to be hb + ep = chl + q + ab + H_2O, responsible for the formation of albite at 6–9 kbar. Albite growing as coarse-grained porphyroblasts may contribute to the abundant fluids that resulted from dehydration reactions and deformation during the formation of the S2 foliation. Thus, it is reasonably clear that the early-phase assemblage cannot be preserved in the matrix.

To investigate the metamorphic evolution of the inferred late-phase assemblage, a P–T pseudosection was calculated in the NCKFMASHTO system using the effective bulk composition generated by excluding garnet (**Figure 9**). The inferred late-phase mineral assemblage is predicted to match the stability field of the assemblage hb + chl + ttn + ep + ab at <9 kbar and 400–500°C. The isopleths of Al^{M2} and Na^{M4} for the measured zoning values of 0.87–0.38 and 0.40–0.22 in magnesio-hornblende yield a P–T vector from ~7.0 kbar/495°C to ~3 kbar/430°C, which is characteristic of cooling decompression. The cooling decompression is predicted to have the rock evolving towards higher water contents (from 1.89 to 2.46 wt%), indicating the infiltration of water during the late-phase metamorphic evolution (Guiraud et al., 2001).

5 ZIRCON U–PB AGE DATA

To obtain the protolith and metamorphism-related ages, the sericite–quartz schist sample EL11, the garnet–mica schist sample EL07 and the granodiorite sample EL12 are for zircon U-Pb dating respectively. Zircon grains in these samples were separated using standard heavy-liquid and magnetic techniques followed by handpicking under a binocular microscope at the Langfang Regional Geological Survey, China. The grains were embedded in epoxy resin discs and polished down to about half-sections to expose the grain interiors. To reveal the internal structures of the zircon grains, cathodoluminescence (CL) images were obtained using a Quanta 200F environmental scanning electron microscope housed at the State Key Laboratory of Orogenic Belts and Crustal Evolution of Peking University. The zircon U–Pb dating was carried out with a quadrupole ICP–MS (Agilient 7500a) connected to an UP-193 Solid-State laser (193 nm, New Wave Research Inc.) at the Ministry of Education Key Laboratory of Orogenic Belts and Crustal Evolution, School of Earth and Space Sciences, Peking University. The laser spot diameters were 25 μm and the laser frequency 10 Hz. The calibrations for the zircon analyses were done using NIST 610 glass as an external standard and Si as an internal standard. The standard zircon 91,500 (1,063 ± 14 Ma, n = 13) was used as an external standard for correcting the effects of U–Pb isotope fractionation. The standard zircon Plesovice (337.3 ± 0.7 Ma) was also used as an external standard to monitor the deviations of age measurements and calculations. The isotopic ratios and elemental contents of the zircons were calculated using GLITTER ver. 4.4 (Van Achterbergh et al., 2001). The concordia ages and diagrams were obtained using Isoplot/Ex (3.0) (Ludwig, 2003). Common lead was corrected using ComPbCorr# (ver. 3.15, Andersen, 2002). The errors given on individual analyses are at the 1σ level, but the weighted mean ages and their errors are reported at the 2σ level. $^{207}Pb/^{206}Pb$ ages were accepted for grains older than 1,000 Ma and $^{206}Pb/^{238}U$ ages for grains younger than 1,000 Ma (Sircombe, 1999). The analytical data are shown in **Supplementary Appendixs S3–S5**.

Zircon grains from sample EL11 are mostly euhedral and subhedral with lengths range from 120 to 80 μm. They mostly show high luminescence and simple oscillatory zoning in the CL images, suggesting their detrital origin mainly from igneous sources (**Figure 10A**). The detrital zircons have concordant ages ranging from 453 ± 9 Ma to 2,583 ± 40 Ma (**Figure 11A**). Four age populations can be discriminated including 2,583–1,532 Ma, 1,401–807 Ma, 701–667 Ma, and 569–453 Ma. Conspicuous age peaks are located at 1,176, 689, and 456 Ma (**Figure 11B**). The youngest coeval zircon grains between 453 ± 9 and 462 ± 5 Ma yield a weighted mean age of 456 ± 5 Ma (MSWD = 0.3, 2σ) which constrains the youngest depositional age of protolith to be 456 ± 5 Ma (**Figure 11A**). It needs to be noted that

some zircons are characterized by metamorphic rims with high luminescence brightness in CL images, however, they were beyond analysis due to the widths of <10 μm.

Zircon grains from sample EL07 are mostly euhedral–subhedral with lengths ranging from 120 to 80 μm. They generally exhibit typical oscillatory or planar zoning with relatively low luminescence brightness in CL images (**Figure 10B**), suggesting their detrital origin was mainly from igneous sources. Most zircons have metamorphic rims with relatively high luminescence brightness, however, they were too narrow for analysis due to the widths of <10 μm. The detrital zircons have a concentrated concordant $^{206}Pb/^{238}U$ age range between 438 ± 6 Ma and 454 ± 6 Ma with Th/U ratios of 0.23–0.97. Thus, we suppose that the protolith of the garnet–mica schist sample is proximal sedimentary rock or volcanic sedimentary rock. The concentrated zircon ages yield a weighted mean $^{206}Pb/^{238}U$ age of 445 ± 2 Ma and MSWD = 0.76 (**Figure 11C**).

Zircon grains from sample EL12 are mostly euhedral–subhedral with lengths ranging from 120 to 80 μm. They generally exhibit typical oscillatory or planar zoning with relatively low luminescence brightness in CL images (**Figure 10C**), suggesting a magmatic origin. Thirty-five analyses show Th/U ratios between 0.39 and 1.18 and define concordant ages which yield a weighted mean $^{206}Pb/^{238}U$ age of 427 ± 2 Ma and MSWD = 0.84 (**Figure 11D**).

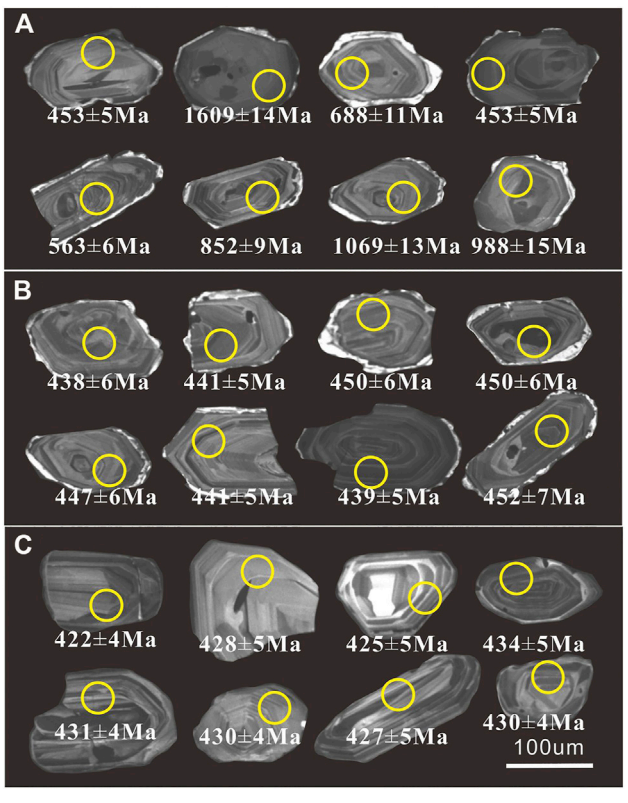

FIGURE 10 | Cathodoluminescence (CL) images of selected zircons from samples EL11 **(A)**, EL07 **(B)**, and EL12 **(C)** at Airgin Sum. Solid circles show positions of LA-ICP-MS analytical sites and ages in Ma.

6 DISCUSSION

6.1 Metamorphic Evolution

Petrographic observations and phase equilibria modelling indicate that both the garnet–phengite schist (EL01) and the garnet–amphibole schist (EL08) record two P/T series of metamorphic evolution including an early high-P/T series and a late medium-P/T series.

6.1.1 The Early-phase HP Evolution

Phase equilibria modelling suggests that both samples underwent a clockwise P–T evolution involving the prograde, peak, and post-peak isothermal decompression stages. The peak conditions were ~18 kbar/~535°C for EL01 and 18 kbar/~500°C for EL08. For both samples, the observed early-phase assemblages cannot match those predicted at their peak conditions because the post-peak decompressional evolution was dominated by dehydration reactions. As indicated in the P–M (H_2O) pseudosections (**Figures 6B**, **8B**), the peak HP minerals of jadeite in EL01 and lawsonite and glaucophane in EL08 could not survive during decompression. Moreover, as the contents of the jadeite and lawsonite reactants would have been rather low, no idiomorphic pseudomorphs of these minerals are likely to be found. Mostly, the metamorphic evolution that was dominated by dehydration in the HP rocks could be triggered by decompression, even with cooling, and in general it will not reach a state of full equilibrium. Thus, in most cases, garnet and phengite can preserve their compositions of the peak condition (or close to it), and their composition isopleths in P–T pseudosections can provide informative peak P–T estimates (Wei and Tian, 2014).

6.1.2 The Late-phase MP Metamorphism

The late-phase metamorphic evolution of samples EL01 and EL08 is characterized by the formation of albite and the S2 foliation. Sample EL01 is characterized by a clockwise P–T vector including a nearly heating path until the P–T condition of ~8 kbar/532°C, constrained by chlorite and muscovite compositions, and a retrograde path of decompression constrained by higher values of X_{An} in the rims of albite porphyroblasts. For sample EL08, only a retrograde path from ~7.0 kbar/495°C to ~3 kbar/430°C with cooling and decompression can be recovered from the Na^{M4} and Al^{M2} isopleths in the hornblende (**Figure 9**), and this needs to be addressed for the genetic connection between the late-phase medium-P/T and the early-phase high-P/T series mineral assemblages. Three vital pieces of evidence are presented. First, the late-phase assemblage in EL01 has a clockwise P–T path, which indicates a complete cycle of compression–exhumation that corresponds to a separate tectonic process. Second, the two-phases of foliation, especially in sample EL08, where the matrix minerals developed an independent foliation and the albite porphyroblasts are observed to be syntectonic, suggest that the early-phase foliation has been displaced. Third, in sample EL01, the formation of the late-phase mineral assemblage with albite requires the ingress of fluids, which is more likely to have

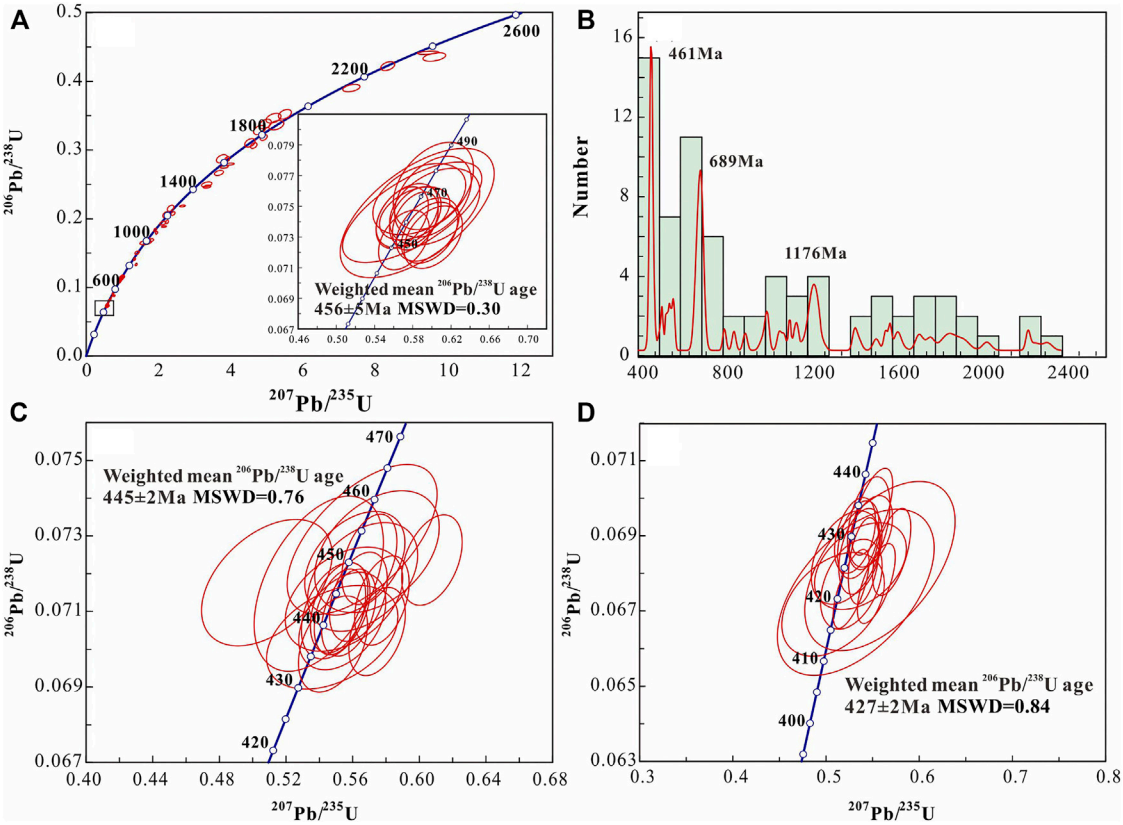

FIGURE 11 | (A) Concordia diagrams showing zircon U-Pb data of sample EL11; **(B)** Relative probability histogram of U–Pb ages of the detrital zircons in sample EL11; **(C)** Concordia diagrams showing detrital zircon U-Pb data in sample EL07; **(D)** Concordia diagrams showing magmatic zircon U-Pb data in sample EL12.

been triggered during the development of the late-phase foliation. As a consequence, we suggest that the late-phase assemblages in the two samples record a metamorphism that overprinted the early-phase HP assemblages, but preceded the later decompressional exhumation. Moreover, the two-phases of metamorphic evolution were accompanied by different foliations, indicating the superimposition of different tectonic activities.

The two phases of metamorphism are suggested to be regional in the studied area as they are consistent to the two phases of deformations (S1 and S2) which are generally observed in the Ondor Sum Group. Due to the modification of the early-phase decompression and late-phase metamorphism, the peak mineral assemblages in the exhumed HP rocks in the Ondor Sum Group mostly failed to be preserved. However, the exception for the garnet–phengite schist and garnet–amphibole schist in the Ondor Sum Group are probably due to the lack of fluid during the metamorphism as indicated above.

6.2 Ages of Protolith and Metamorphism of the Ondor Sum Group in Argin Sum

Different ages were abtained in the Ondor Sum Group in the previous research. In Wulangou, meta-andesites of arc type yielded a protolith age of 470 ± 2 Ma using the zircon U–Pb method (Li et al., 2012), and sodic amphibole from the blueschists and phengite from the quartz schists yielded $^{40}Ar/^{39}Ar$ ages of 426 ± 15 and 454–453 Ma, respectively (Tang and Yan, 1993; De Jong et al., 2006). At Naomuhunni, an epidote–blueschist block reported by Xu et al. (2001) yielded a glaucophane $^{40}Ar/^{39}Ar$ age of 383 ± 13 Ma.

Comparison of zircon age spectrum (**Figure 12**) shows that the detrital zircon ages of the HP schist samples at Airgin Sum are consistent with those at Naomuhunni, both of which belong to the northern Ondor Sum Group in NOB. Moreover, they are consistent with the age patterns of the Mongolia and the northeastern China plot. Their zircon ages suggest multiple sources contributed to the sediment formation. For instance, the major age peak at 456–442 Ma are supposed to reflect the early Paleozoic arc magmatism in the XIMOB (Chen et al., 2000; Shi et al., 2003; Jian et al., 2008; Chen et al., 2009; Xue et al., 2009; Li et al., 2012). The age groups with peaks of ~689 and ~1,176 Ma are consistent with those reported in the Ergun and Xing' an blocks (Zhou and Wilde (2013); Zhou et al., 2014) and the Southern Mongolian block (Badarch et al., 2002; Yarmolyuk et al., 2005). And the other older ages should be derived from the North China Craton (NCC, Zhao et al., 2001; Zhao et al., 2002; Wilde et al., 2002). The age groups of the Ondor Sum

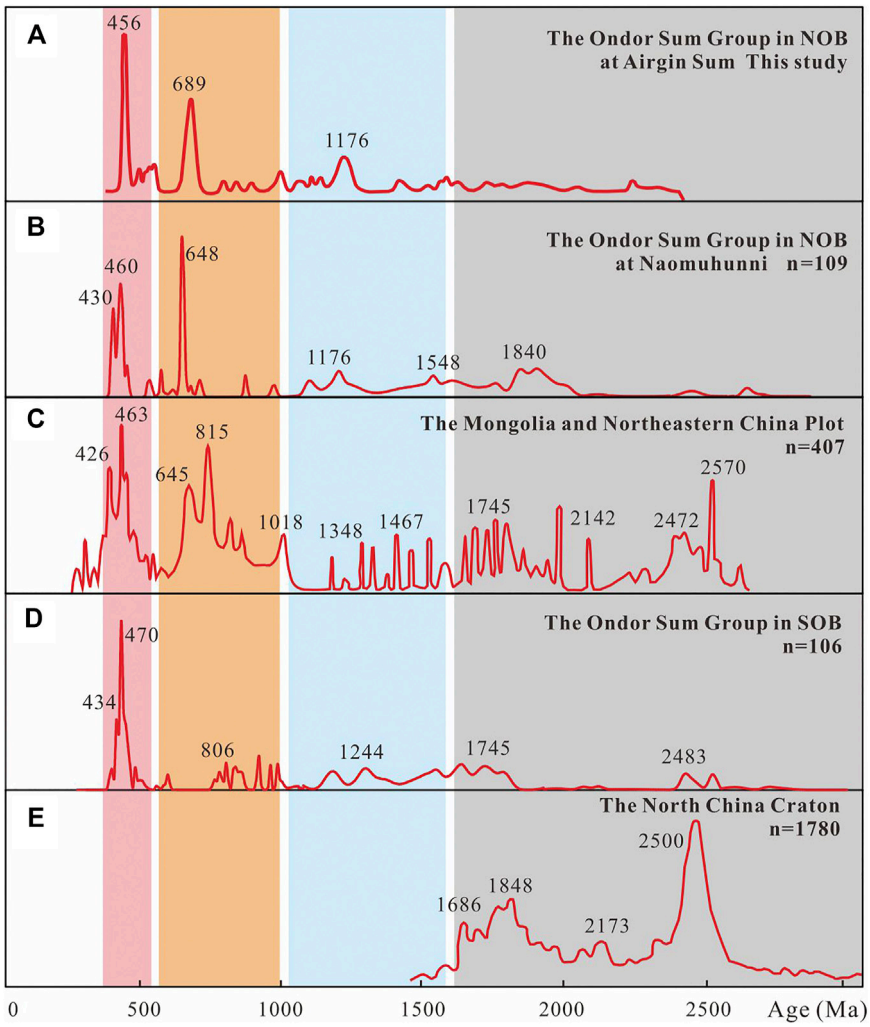

FIGURE 12 | Relative probability diagrams showing age distribution of Ondor Sum Group in central Inner Mongolia **(A,B,D)**, the Mongolia and Northeastern China Plot **(C)** and the NCC **(E)**. Data are cited from Zhou and Wilde (2013), Zhou et al. (2014), Xu et al. (2013, 2014), and Rojas-Agramonte et al. (2011).

Group in the SOB are mostly the same as the NOB except a conspicuous absence of ~689 Ma peak and ~1,176 Ma, which is probably attributed to the absence or decrease of detrital contribution from the blocks in the north.

No available metamorphic age data have been obtained in the samples, which, however, can be alternatively constrained between ca. 442 and ca. 425 Ma, on the basis of the youngest detrital age group of ca. 442 Ma and the ages of ca. 425 Ma for the granodiorite intrusions. This estimate is consistent with the reported $^{40}Ar/^{39}Ar$ ages of 454–453 Ma in the phengite schist (De Jong et al., 2006) and $^{40}Ar/^{39}Ar$ age of ~426 Ma in the blueschist in Ondor Sum Group (Tang and Yan, 1993). It needs to be noted that the glaucophane $^{40}Ar/^{39}Ar$ age of 383 ± 13 Ma was obtained in the blueschists in Ondor Sum Group (Xu et al., 2001). Based on the two phases of metamorphic evolution indicated above, we suggest, therefore, that the metamorphic age of 383 ± 13 Ma records the overprinting of the late-phase medium-P/T series metamorphism and not the early-phase high-P/T series metamorphism. In the context of the geological setting, this age seems to be consistent with the 399 ± 8 Ma age of the Barrovian metamorphic belt within the limit of error.

6.3 Geological Implication for the Metamorphism

As indicated above, the HP rocks exhumed from ancient subduction zones have been controversially argued to record much warmer geotherms than numerical modelling results.

Although the Syracuse models were argued to have underestimated the temperatures of subduction zones, they have been well matched by the peak P–T conditions reported for the exhumed HP rocks (Brown and Johnson, 2018), including those of the Franciscan at Jenner, United States (Krogh Ravna and Terry, 2004), southwest Tianshan belt (Wei C. J. et al., 2009;

Tian and Wei, 2013), the north Qilian belt (Wei C. J. et al., 2009), and the Yuli belt in China (Huang et al., 2021). The numerical modelling results of Syracuse et al. (2010) seem to be well consistent with the records from natural HP rocks if their peak pressure conditions are well recovered.

The investigated garnet–phengite schist (EL01) and garnet–amphibole schist (EL08) in the Ondor Sum Group are interpreted to have experienced HP metamorphism along clockwise P–T paths in the early phase, with a thermal gradient of 8°C/km at peak conditions, and they can be classified as typical high-P/T types (**Figure 13**). According to the numerical modelling of Syracuse et al. (2010), the prograde P–T paths are apparently warmer than those in most subduction zones. Thermal structure of subduction zones is controlled by various factors including the age of subducted oceanic crust, the convergent rate, the subduction dip angle and the thicknesses of both subducting and overriding lithospheres (Kirby et al., 1991; van Hunen et al., 2002; Gerya and Meilick, 2011; van Keken et al., 2011; Leng and Mao, 2015). Nevertheless, on the context of field tectonic evolution, the HP schists of the Ondor Sum Group at Airgin Sum seem to be related to a warm subduction at the terminal evolution of the Paleo-Asian Ocean, which we suggest may correspond to the subduction of a young slab (Syracuse et al., 2010), or a low-rate of subduction (<2 cm/yr, van Keken et al., 2002). This interpretation is suggested by several lines of evidence, including: 1) the protoliths of the metabasite in this study showing affinities between N-MORB and E-MORB which has been previously suggested to represent environment of limited intercontinental ocean basins (Zhang et al., 2014), 2) the high P/T metamorphism in the garnet–phengite schist which has occurred soon after formation of the protolith; 3) the absence of arc magmatic activity since ~420 Ma which probably indicates termination of subduction process (Song et al., 2015). The P–T conditions of the late-phase metamorphism that was overprinted on our HP schist sample EL08 indicate a thermal gradient of 22–25°C/km, which is typical of the medium-P/T facies series (Miyashiro, 1994). We suppose that the late-phase metamorphism is consistent with the metamorphism of the Baoyintu Group, in which the near-peak of a typical medium-P/T Barrovian metamorphism took place at 399 ± 8 Ma, corresponding to an orogenic thickening process (Chen et al., 2015). This sequence of events can be supported by other lines of evidence, including: 1) the development of the Upper Devonian molasses formation that unconformably overlies early Paleozoic mélanges and flysch in both the NOB and SOB (Xu et al., 2013), 2) the gap in magmatic activity between 420 and 360 Ma (Xu et al., 2013; Song et al., 2015), corresponding to the collisional orogeny and 3) the development of collision-related biotite monzogranites of high-K calc-alkaline series of 423–392 Ma in Sunidzuoqi and Xilinhot (Shi et al., 2004; Xu et al., 2015).

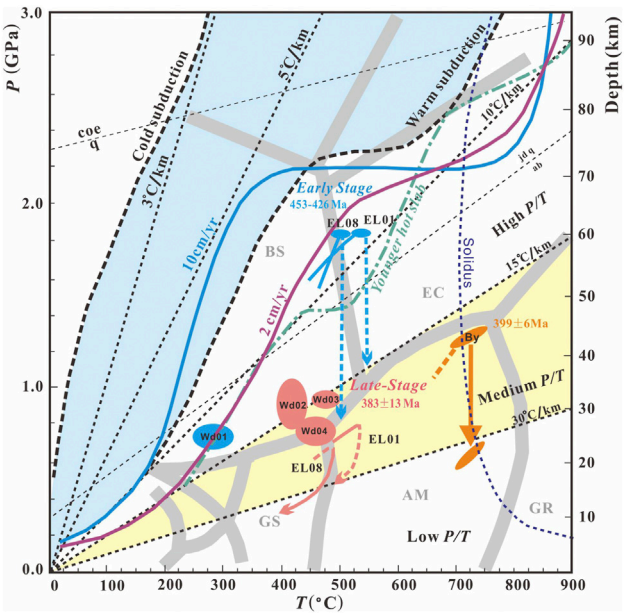

FIGURE 13 | The summarized P–T conditions and paths of the high-pressure rocks in the Ondor Sum Group. Wd01 refer to the P–T results of the blueschist at Wulangou cited from Tang and Yan (1993). Wd02 and Wd03 refer to the P–T results of sodic-amphibolite bearing quartzite (Li et al., 2014b) and barroisite schist (Zhang et al., 2015) at Airgin Sum respectively. Wd04 refer to the P–T result of epidote-blueschist at Naomuhunni (Zhang et al., 2015). By refers to the P–T path of the Barrovian metamorphism the Baoyintu Group in Chen et al. (2015). EL01 and EL08 refer to the P–T paths of HP schists in this study. The bold dotted curves indicate the approximate range of the geothermal gradient at slab surface between cold and hot subduction zones simulated in Syracuse et al. (2010). The thick curves indicate P–T paths predicted for differing convergence velocities of the incoming plate (van Keken et al., 2002, 20 Ma, 30 dip). In general, slower convergence velocities (2 cm/yr) are predicted to result in higher temperatures at a given depth compared to faster convergence velocities (van Keken et al., 2002, 10 cm/yr). The thick chain-dotted line refers to a younger slab have higher geothermal gradients at both the surface as indicated in Wei and Zheng et al. (2020). The reaction ab = jd + q and the transition lines of Al_2SiO_5 were calculated using THERMOCALC. The division of the metamorphic facies series is after Miyashiro (1961, 1994). The metamorphic facies boundaries are after Maruyama et al. (1996) and Oh and Liou (1998).

Consequently, a preliminary tectonic reconstruction may be achieved for the evolution of the Paleo-Asian Ocean in central Inner Mongolia although our results are temporarily representative of a local area and more researches are still needed. The Paleo-Asian Ocean was initiated at ca. 500 Ma in central Inner Mongolia with bidirectional subduction, both northward beneath the Southern Mongolia Block (SMB) and southward beneath the NCC (e.g., Xiao et al., 2003; Xu et al., 2013; Song et al., 2015). This resulted in the formation of the 499–425 Ma Bainaimiao Arc complexes in the south and the 482–428 Ma Baolidao Arc complexes in the north, as well as contemporaneous high-P/T mélanges represented by the Ondor Sum Group. From ~420 Ma, the Paleo-Asian oceanic system came to an end and collision resulted in orogenic processes. The Ondor Sum Group at Airgin Sum was supposed to be involved in the collision with overprinting by the medium-P/T metamorphism. We thus suggest that the HP schists of the Ondor Sum Group at Airgin Sum record the tectonic transition from terminal subduction of the Paleo-Asian Ocean to continental collision.

7 CONCLUSION

Our field observations, petrographic observations, phase equilibria modelling, and zircon U–Pb dating for the samples of Ondor Sum Group in the Airgin Sum area, have led to the following conclusions:

1) Both HP schists record two phases of metamorphism and two phases of foliation development, based on their mineral assemblages and petrography.

2) Both phases of metamorphism were characterized by clockwise P–T evolutions involving pre-peak prograde, peak, and post-peak decompression stages. The peak P–T conditions of the early phase were ~18 kbar/~535°C for sample EL01 and 18 kbar/~500°C for EL08, and the modeled peak mineral assemblage that contained jadeite, lawsonite, and glaucophane could not survive the isothermal decompression, which was dominated by dehydration reactions. The peak P–T conditions of the late-phase metamorphism were ~8 kbar/532°C and ~7.0 kbar/495°C, respectively, and this metamorphism overprinted the early-phase metamorphism.

3) Available zircon ages data suggest that the early-phase HP metamorphism occurs in the early Paleozoic.

4) The data for the two phases of metamorphism indicate two entirely different P/T series, an early high-P/T series with a thermal gradient of ~8°C/km, pointing to the subduction of a warm subduction enviroment, and a late medium-P/T series with a geothermal gradient of 22–25°C/km that was related to collisional thickening of the crust. We suggest that the early high-P/T metamorphism represents the terminal subduction of the Paleo-Asian oceanic plate, and that the later medium-P/T metamorphism represents the involvement of these schists in the continental collision that took place after the closure of the Paleo-Asian Ocean in the Devonian.

DATA AVAILABILITY STATEMENT

The original contributions presented in the study are included in the article/**Supplementary Material**, further inquiries can be directed to the corresponding author.

AUTHOR CONTRIBUTIONS

JZ: Methodology, Software, Writing Original Draft, Resourses, Formal analysis, Validation. WX, CW: Conceptualization. HC, LJ: Investigation. ST: Data Curation.

FUNDING

This work was financially supported by the National Natural Science Foundation of China (Grant Numbers 42072073 and 41702049), Opening Foundation of Key Laboratory of Mineral Resources Evaluation in Northeast Asia, Ministry of Natural Resources (DBY-ZZ-19-08), the Major State Basic Research Development Program of China (2013CB429801), and the China Survey of Geology (121201091100).

ACKNOWLEDGMENTS

We thank Bei Xu and Pohung Huang for their constructive comments of the manuscript, and thank Hong Qing and Xiaoli Li for their help in experimental analyses. We also thank anonymous reviewers for their thoughtful and constructive reviews on the manuscript.

SUPPLEMENTARY MATERIAL

The Supplementary Material for this article can be found online at: https://www.frontiersin.org/articles/10.3389/feart.2022.817682/full#supplementary-material

REFERENCES

Agard, P., Plunder, A., Angiboust, S., Bonnet, G., and Ruh, J. (2018). The Subduction Plate Interface: Rock Record and Mechanical Coupling (From Long to Short Timescales). *Lithos* 320-321, 537–566. doi:10.1016/j.lithos.2018.09.029

Andersen, T. (2002). Correction of Common lead in U-Pb Analyses that Do Not Report 204Pb. *Chem. Geology.* 192, 59–79. doi:10.1016/s0009-2541(02)00195-x

Badarch, G., Dickson Cunningham, W., and Windley, B. F. (2002). A New Terrane Subdivision for Mongolia: Implications for the Phanerozoic Crustal Growth of Central Asia. *J. Asian Earth Sci.* 21, 87–110. doi:10.1016/s1367-9120(02)00017-2

Brown, M., and Johnson, T. (2018). Secular Change in Metamorphism and the Onset of Global Plate Tectonics. *Am. Mineral.* 103 (2), 181–196. doi:10.2138/am-2018-6166

Carson, C. J., Powell, R., and Clarke, G. L. (1999). Calculated mineral Equilibria for Eclogites in $CaO-Na_2O-FeO-MgO-Al_2O_3-SiO_2-H_2o$: Application to the Pouébo Terrane, Pam Peninsula, New Caledonia. *J. Metamorphic Geology.* 17, 9–24. doi:10.1046/j.1525-1314.1999.00177.x

Chen, B., Jahn, B.-m., Wilde, S., and Xu, B. (2000). Two Contrasting Paleozoic Magmatic Belts in Northern Inner Mongolia, China: Petrogenesis and Tectonic Implications. *Tectonophysics* 328, 157–182. doi:10.1016/s0040-1951(00)00182-7

Chen, B., Jahn, B. M., and Tian, W. (2009). Evolution of the Solonker Suture Zone: Constraints from Zircon U-Pb Ages, Hf Isotopic Ratios and Whole-Rock Nd-Sr Isotope Compositions of Subduction- and Collision-Related Magmas and Forearc Sediments. *J. Asian Earth Sci.* 34, 245–257. doi:10.1016/j.jseaes.2008.05.007

Chen, C., Zhang, Z., Guo, Z., Li, J., Feng, Z., and Tang, W. (2012). Geochronology, Geochemistry, and its Geological Significance of the Permian Mandula Mafic Rocks in Damaoqi, Inner Mongolia. *Sci. China Earth Sci.* 55, 39–52. doi:10.1007/s11430-011-4277-z

Chen, Y., Wei, C., Zhang, J., and Chu, H. (2015). Metamorphism and Zircon U-Pb Dating of Garnet Amphibolite in the Baoyintu Group, Inner Mongolia. *Sci. Bull.* 60, 1698–1707. doi:10.1007/s11434-015-0890-0

Chu, H., Zhang, J., Wei, C., Wang, H., and Ren, Y. (2013). A New Interpretation of the Tectonic Setting and Age of Meta-Basic Volcanics in the Ondor Sum Group, Inner Mongolia. *Chin. Sci. Bull.* 58, 3580–3587. doi:10.1007/s11434-013-5862-7

Coggon, R., and Holland, T. J. B. (2002). Mixing Properties of Phengitic Micas and Revised Garnet-Phengite Thermobarometers. *J. Metamorph Geol.* 20, 683–696. doi:10.1046/j.1525-1314.2002.00395.x

De Jong, K., Xiao, W., Windley, B. F., Masago, H., and Lo, C.-h. (2006). Ordovician $^{40}Ar/^{39}Ar$ Phengite Ages from the Blueschist-Facies Ondor Sum Subduction-Accretion Complex (Inner Mongolia) and Implications for the Early Paleozoic History of continental Blocks in China and Adjacent Areas. *Am. J. Sci.* 306, 799–845. doi:10.2475/10.2006.02

Diener, J. F. A., Powell, R., White, R. W., and Holland, T. J. B. (2007). A New Thermodynamic Model for Clino- and Orthoamphiboles in the System Na_2O–CaO–FeO–MgO–Al_2O_3–SiO_2–H_2O–O. *J. Metamorph. Geol.* 25, 631–656. doi:10.1111/j.1525-1314.2007.00720.x

Gerya, T. V., and Meilick, F. I. (2011). Geodynamic Regimes of Subduction Under an Active Margin: Effects of Rheological Weakening by Fluids and Melts. *J. Metamorph. Geol.* 29 (1), 7–31. doi:10.1111/j.1525-1314.2010.00904.x

Green, E. C. R., White, R. W., Diener, J. F. A., Powell, R., Holland, T. J. B., and Palin, R. M. (2016). Activity-composition Relations for the Calculation of Partial Melting Equilibria in Metabasic Rocks. *J. Metamorph. Geol.* 34, 845–869. doi:10.1111/jmg.12211

Groppo, C., Beltrando, M., and Compagnoni, R. (2009). TheP-Tpath of the Ultra-high Pressure Lago Di Cignana and Adjoining High-Pressure Meta-Ophiolitic Units: Insights into the Evolution of the Subducting Tethyan Slab. *J. Metamorph. Geol.* 27 (3), 207–231. doi:10.1111/j.1525-1314.2009.00814.x

Guiraud, M., Powell, R., and Rebay, G. (2001). H2 O in Metamorphism and Unexpected Behaviour in the Preservation of Metamorphic mineral Assemblages. *J. Metamorph. Geol.* 19, 445–454. doi:10.1046/j.0263-4929.2001.00320.x

Hernández–Uribe, D., Mattinson, C. G., and Zhang, J. X. (2018). Phase Equilibrium Modelling and Implications for P –T Determinations of Medium-temperature UHP Eclogites, North Qaidam Terrane, China. *J. Metamorph. Geol.* 36 (9), 1237–1261. doi:10.1111/jmg.12444

Holder, R. M., Viete, D. R., Brown, M., and Johnson, T. E. (2019). Metamorphism and the Evolution of Plate Tectonics. *Nature* 572 (7769), 378–381. doi:10.1038/s41586-019-1462-2

Holland, T. J. B., and Powell, R. (1998). An Internally Consistent Thermodynamic Data Set for Phases of Petrological Interest. *J. Metamorph. Geol.* 16, 309–343.

Holland, T., and Powell, R. (2003). Activity?composition Relations for Phases in Petrological Calculations: an Asymmetric Multicomponent Formulation. *Contrib. Mineral. Petrol.* 145, 492–501. doi:10.1007/s00410-003-0464-z

Holland, T. J. B., and Powell, R. (2011). An Improved and Extended Internally Consistent Thermodynamic Dataset for Phases of Petrological Interest, Involving a New Equation of State for Solids. *J. Metamorph. Geol.* 29, 333–383. doi:10.1111/j.1525-1314.2010.00923.x

Huang, P. H., Wei, C., and Zhang, J. (2021). High- P Metamorphism of Garnet-Epidote-Amphibole Schists from the Yuli Belt, Eastern Taiwan: Evidence Related to Warm Subduction. *J. Metamorph. Geol.* 39, 675–693. doi:10.1111/jmg.12577

IMBGMR (Inner Mongolian Bureau of Geology and Mineral Resources) (1991). *Regional Geology of Inner Mongolian Autonomous Region*. Beijing: Geological Publishing House, 726. (in Chinese with English abstract).

Jian, P., Liu, D., Kröner, A., Windley, B. F., Shi, Y., Zhang, F., et al. (2008). Time Scale of an Early to Mid-paleozoic Orogenic Cycle of the Long-Lived Central Asian Orogenic Belt, Inner Mongolia of China: Implications for Continental Growth. *Lithos* 101, 233–259. doi:10.1016/j.lithos.2007.07.005

Jian, P., Liu, D., Kröner, A., Windley, B. F., Shi, Y., Zhang, W., et al. (2010). Evolution of a Permian Intraoceanic Arc-Trench System in the Solonker Suture Zone, Central Asian Orogenic Belt, China and Mongolia. *Lithos* 118, 169–190. doi:10.1016/j.lithos.2010.04.014

Jian, P., Kröner, A., Windley, B. F., Shi, Y., Zhang, W., Zhang, L., et al. (2012). Carboniferous and Cretaceous Mafic-Ultramafic Massifs in Inner Mongolia (China): A SHRIMP Zircon and Geochemical Study of the Previously Presumed Integral "Hegenshan Ophiolite". *Lithos* 142-143, 48–66. doi:10.1016/j.lithos.2012.03.007

Zhang, J., Wei, C., and Chu, H. (2015). Blueschist Metamorphism and its Tectonic Implication of Late Paleozoic-Early Mesozoic Metabasites in the Mélange Zones, central Inner Mongolia, China. *J. Asian Earth Sci.* 97, 352–364. doi:10.1016/j.jseaes.2014.07.032

Kirby, S. H., Durham, W. B., and Stern, L. A. (1991). Mantle Phase Changes and Deep-Earthquake Faulting in Subducting Lithosphere. *Science* 252 (5003), 216–225. doi:10.1126/science.252.5003.216

Kohn, M. J., Castro, A. E., Kerswell, B. C., Ranero, C. R., and Spear, F. S. (2018). Shear Heating Reconciles thermal Models with the Metamorphic Rock Record of Subduction. *Proc. Natl. Acad. Sci. USA* 115 (46), 11706–11711. doi:10.1073/pnas.1809962115

Krogh, E. J., and Råheim, A. (1978). Temperature and Pressure Dependence of Fe-Mg Partitioning between Garnet and Phengite, with Particular Reference to Eclogites. *Contr. Mineral. Petrol.* 66, 75–80. doi:10.1007/bf00376087

Krogh Ravna, E. J., and Terry, M. P. (2004). Geothermobarometry of UHP and HP Eclogites and Schists - an Evaluation of Equilibria Among Garnet-Clinopyroxene-Kyanite-Phengite-Coesite/quartz. *J. Metamorph. Geol.* 22 (6), 579–592. doi:10.1111/j.1525-1314.2004.00534.x

Leake, B., Woolley, A., Arps, C., Birch, W., Gilbert, M., Grice, J., et al. (1997). Nomenclature of Amphiboles: Report of the Subcommitee on Amphiboles of the International Mineralogical Association, Commission on New Minerals and Mineral Names. *Can. Mineral.* 35, 219–246.

Leng, W., and Mao, W. (2015). Geodynamic Modeling of thermal Structure of Subduction Zones. *Sci. China Earth Sci.* 58, 1070–1083. doi:10.1007/s11430-015-5107-5

Li, J. Y., Gao, L. M., and Sun, G. H. (2007). Shuangjingzi Middle Triassic Syn-Collisional Crust-Derived Granite in the East Inner Mongolia and its Constraint on the Timing of Collision between Siberian and Sino-Korean Paleo-Plates (In Chinese). *Acta Geol. Sin.* 23, 565–582. doi:10.1631/jzus.2007.B0900

Li, C. D., Zhao, L. G., Wang, H. C., Zhang, K., Xu, Y. W., Gu, C. Y., et al. (2012). LA-ICP MS U-Pb Geochronology of Zircons from the Wenduermiao Group and its Tectonic Significance. *Acta Petrol. Sin.* 28, 3705–3714. (in Chinese with English abstract).

Li, R. B., Xu, B., Zhao, P., Tong, Q. L., and Zhang, J. R. (2014). The Discovery of Blueschist-Facies Rock in Airgin Sum Area, Erenhot, Inner Mongolia and its Tectonic Significance. *Chin. Sci. Bull.* 59, 66–71. doi:10.1360/972012-1670

Liou, J. G., Maruyama, S., and Cho, M. (1987). Very Low-Grade Metamorphism of Vocanic and Volcaniclastic Rocks-mineral Assemblages and mineral Facies. *Low Temper. Metamorph.* 59, 113.

Liu, D. Y., Jian, P., Zhang, Q., Zhang, F., Shi, Y., Shi, G., et al. (2003). SHRIMP Dating of Adakites in the Tulinkai Ophiolite, Inner Mongolia: Evidence for the Early Paleozoic Subduction. *Acta Geol. Sin.* 77, 317–326.

Liu, W., Siebel, W., Li, X.-j., and Pan, X.-f. (2005). Petrogenesis of the Linxi Granitoids, Northern Inner Mongolia of China: Constraints on Basaltic Underplating. *Chem. Geology.* 219, 5–35. doi:10.1016/j.chemgeo.2005.01.013

Liu, J. F., Chi, X. G., Zhang, X. Z., Ma, Z. H., Zhao, Z., Wang, T. F., et al. (2009). Geochemical Characteristic of Carboniferous Quartzdiorite in the Southern Xiwuqi Area, Inner Mongolia and its Tectonic Significance. *Acta Geol. Sin.* 83, 365–376. (in Chinese with English abstract). doi:10.1016/S1874-8651(10)60080-4

Liu, J., Li, J., Chi, X., Qu, J., Hu, Z., Fang, S., et al. (2012). A Late-Carboniferous to Early Early-Permian Subduction–Accretion Complex in Daqing Pasture, southeastern Inner Mongolia: Evidence of Northward Subduction beneath the Siberian Paleoplate Southern Margin. *Lithos* 177, 285–296. doi:10.1016/j.lithos.2013.07.008

Ludwig, K. R. (2003). *ISOPLOT 3.0: A Geochronological Toolkit for Microsoft Excel*, Vol. 4. Berkeley, CA: Berkeley Geochronology Center Special Publication.

Maruyama, S., Liou, J. G., and Terabayashi, M. (1996). Blueschists and Eclogites of the World and Their Exhumation. *Int. Geol. Rev.* 38 (6), 485–594. doi:10.1080/00206819709465347

Maresch, W. V. (1977). Experimental Studies on Glaucophane: an Analysis of Present Knowledge. *Tectonophysics* 43, 109–125. doi:10.1016/0040-1951(77)90008-7

Miao, L., Fan, W., Liu, D., Zhang, F., Shi, Y., and Guo, F. (2008). Geochronology and Geochemistry of the Hegenshan Ophiolitic Complex: Implications for Late-Stage Tectonic Evolution of the Inner Mongolia-Daxinganling Orogenic Belt, China. *J. Asian Earth Sci.* 32, 348–370. doi:10.1016/j.jseaes.2007.11.005

Miyashiro, A. (1961). Evolution of Metamorphic Belts. *J. Petrol.* 2 (3), 277–311. doi:10.1093/petrology/2.3.277

Miyashiro, A. (1994). *Metamorphic Petrology*. London: UCL Press Limited.

Oh, C. W., and Liou, J. G. (1998). A Petrogenetic Grid for Eclogite and Related Facies Under High-Pressure Metamorphism. *Island Arc* 7 (1-2), 36–51. doi:10.1046/j.1440-1738.1998.00180.x

Peacock, S. M., and Wang, K. (1999). Seismic Consequences of Warm versus Cool Subduction Metamorphism: Examples from Southwest and Northeast Japan. *Science* 286 (5441), 937–939. doi:10.1126/science.286.5441.937

Peacock, S. M. (1996). Thermal and Petrologic Structure of Subduction Zones. *Subduction: Top. Bottom* 96, 119–133.

Penniston-Dorland, S. C., Kohn, M. J., and Manning, C. E. (2015). The Global Range of Subduction Zone thermal Structures from Exhumed Blueschists and Eclogites: Rocks Are Hotter Than Models. *Earth Planet. Sci. Lett.* 428, 243–254. doi:10.1016/j.epsl.2015.07.031

Qiao, X., Li, W., Zhong, R., Hu, C., Zhu, F., and Li, Z. (2017). Elemental and Sr-Nd Isotopic Geochemistry of the Uradzhongqi Magmatic Complex in Western Inner Mongolia, China: A Record of Early Permian post-collisional Magmatism. *J. Asian Earth Sci.* 144, 171–183. doi:10.1016/j.jseaes.2016.12.002

Rojas-Agramonte, Y., Kröner, A., Demoux, A., Xia, X., Wang, W., Donskaya, T., et al. (2011). Detrital and Xenocrystic Zircon Ages from Neoproterozoic to Palaeozoic Arc Terranes of Mongolia: Significance for the Origin of Crustal Fragments in the Central Asian Orogenic Belt. *Gondwana Res.* 19, 751–763. doi:10.1016/j.gr.2010.10.004

Shi, G., Liu, D., Zhang, F., Jian, P., Miao, L., Shi, Y., et al. (2003). SHRIMP U-Pb Zircon Geochronology and its Implications on the Xilin Gol Complex, Inner Mongolia, China. *Chin. Sci. Bull.* 48, 2742–2748. doi:10.1016/j.sedgeo.2003.12.012

Shi, Y. R., Liu, D. Y., Zhang, Q., Zhang, F. Q., Miao, L. C., Shi, G. H., et al. (2004). SHRIMP Dating of Diorites and Granites in Southern Suzuoqi, Inner Mongolia. *Acta Geol. Sin.* 78, 789–799. (in Chinese with English abstract). doi:10.1007/BF02873097

Shi, Y. R., Liu, D. Y., Zhang, Q., Jiang, P., Zhang, F. Q., Miao, L. C., et al. (2005). The Petrogenesis and SHRIMP Dating of the Baiyinbaolidao Adakitic Rocks in Southern Suzuoqi, Inner Mongolia. *Acta Petrol. Sin.* 21, 143–150. (in Chinese with English abstract).

Sircombe, K. N. (1999). Tracing Provenance through the Isotope Ages of Littoral and Sedimentary Detrital Zircon, Eastern Australia. *Sediment. Geology.* 124, 47–67. doi:10.1016/s0037-0738(98)00120-1

Song, S. G., Wang, M. M., Xu, X., Wang, C., Niu, Y. L., and Allen, M. B. (2015). Ophiolites in the Xing'an-Inner mongolia Accretionary belt of the CAOB: Implications for Two Cycles of Seafloor Spreading and Accretionary Orogenic Events. *Tectonics* 34, 1371–1385. doi:10.1002/2015tc003948

Sun, L. X., Ren, B. F., Zhao, F. Q., Gu, Y. C., Li, Y. F., and Liu, H. (2013). Zircon U-Pb Dating and Hf Isotopic Compositions of the Mesoporterozoic Granitic Gneiss in Xilinhot Block, Inner Mongolia. *Geol. Bull. China* 32, 327–340.

Syracuse, E. M., van Keken, P. E., and Abers, G. A. (2010). The Global Range of Subduction Zone thermal Models. *Phys. Earth Planet. Interiors* 183 (1–2), 73–90. doi:10.1016/j.pepi.2010.02.004

Tamblyn, R., Zack, T., Schmitt, A. K., Hand, M., Kelsey, D., Morrissey, L., et al. (2019). Blueschist from the Mariana Forearc Records Long-Lived Residence of Material in the Subduction Channel. *Earth Planet. Sci. Lett.* 519, 171–181. doi:10.1016/j.epsl.2019.05.013

Tang, K., and Yan, Z. (1993). Regional Metamorphism and Tectonic Evolution of the Inner Mongolian Suture Zone. *J. Metamorphic Geology.* 11, 511–522.

Tang, K. D., Yan, Z. J., Zhang, R. P., Xu, D. K., Tchi, Y., Su, Y. Z., et al. (1983). On Wentermiao Group and its Tectonic Significance. *Contrib. Project Plate Tectonic North. China* 1, 186–208. (in Chinese).

Tang, K. (1990). Tectonic Development of Paleozoic Foldbelts at the north Margin of the Sino-Korean Craton. *Tectonics* 9, 249–260. doi:10.1029/tc009i002p00249

Tian, Z. L., and Wei, C. J. (2013). Metamorphism of Ultrahigh-Pressure Eclogites from the Kebuerte Valley, South Tianshan, NW China: Phase Equilibria and P-T Path. *J. Metamorph. Geol.* 31, 281–300. doi:10.1111/jmg.12021

Tong, Y., Jahn, B.-m., Wang, T., Hong, D.-w., Smith, E. I., Sun, M., et al. (2015). Permian Alkaline Granites in the Erenhot-Hegenshan belt, Northern Inner Mongolia, China: Model of Generation, Time of Emplacement and Regional Tectonic Significance. *J. Asian Earth Sci.* 97, 320–336. doi:10.1016/j.jseaes.2014.10.011

Tsujimori, T., and Ernst, W. G. (2014). Lawsonite Blueschists and Lawsonite Eclogites as Proxies for Palaeo-Subduction Zone Processes: a Review. *J. Meta. Geol.* 32 (5), 437–454. doi:10.1111/jmg.12057

Tsujimori, T., Sisson, V., Liou, J., Harlow, G., and Sorensen, S. (2006). Very-low-temperature Record of the Subduction Process: A Review of Worldwide Lawsonite Eclogites. *Lithos* 92, 609–624. doi:10.1016/j.lithos.2006.03.054

Van Achterbergh, E., Ryan, C., Jackson, S., and Griffin, W. L. (2001). *Data Reduction Software for LA-ICP-MS in Laser-Ablation-ICP MS in the Earth Sciences*. Editor P. Sylvester (Sylvester: Mineralogical Association of Canada Short Course), 29, 239–243.

van Hunen, J., van den Berg, A. P., and Vlaar, N. J. (2002). On the Role of Subducting Oceanic Plateaus in the Development of Shallow Flat Subduction. *Tectonophysics* 352, 317–333. doi:10.1016/s0040-1951(02)00263-9

van Keken, P. E., Hacker, B. R., Syracuse, E. M., and Abers, G. A. (2011). Subduction Factory: 4. Depth-dependent Flux of H_2O from Subducting Slabs Worldwide. *J. Geophys. Res.-Solid Earth*, 116. doi:10.1029/2010jb007922

van Keken, P. E., Wada, I., Abers, G. A., Hacker, B. R., and Wang, K. (2018). Mafic High-Pressure Rocks Are Preferentially Exhumed from Warm Subduction Settings. *Geochem. Geophys. Geosyst.* 19 (9), 2934–2961. doi:10.1029/2018gc007624

van Keken, P. E., Wada, I., Sime, N., and Abers, G. A. (2019). Thermal Structure of the Forearc in Subduction Zones: A Comparison of Methodologies. *Geochem. Geophys. Geosyst.* 20, 3268–3288. doi:10.1029/2019gc008334

Wang, X. C., Wilde, S. A., Xu, B., and Pang, C. J. (2015). Origin of Arc-like continental Basalts: Implications for Deep-Earth Fluid Cycling and Tectonic Discrimination. *Lithos* 261, 5–45.

Wei, C. J., and Clarke, G. L. (2011). Calculated Phase Equilibria for MORB Compositions: a Reappraisal of the Metamorphic Evolution of Lawsonite Eclogite. *J. Metamorph. Geol.* 29 (9), 939–952. doi:10.1111/j.1525-1314.2011.00948.x

Wei, C., and Tian, Z. (2014). Modelling of the Phase Relations in High-Pressure and Ultrahigh-Pressure Eclogites. *Isl. Arc.* 23 (4), 254–262. doi:10.1111/iar.12087

Wei, C. J., and Zheng, Y. F. (2020). Metamorphism, Fluid Behavior and Magmatism in Oceanic Subduction Zones. *Sci. China (Earth Sciences)* 63 (01), 56–81. doi:10.1007/s11430-019-9482-y

Wei, C. J., Wang, W., Clarke, G., Zhang, L. F., and Song, S. G. (2009a). Metamorphism of High/ultra-High-Pressure Pelitic–Felsic Schist in the South Tianshan Orogen, NW China: Phase Equilibria and P-T Path. *J. Petrol.* 50, 1973–1991. doi:10.1093/petrology/egp064

Wei, C. J., Yang, Y., Su, X. L., Song, S. G., and Zhang, L. F. (2009b). Metamorphic Evolution of Low-Teclogite from the North Qilian Orogen, NW China: Evidence from Petrology and Calculated Phase Equilibria in the System NCKFMASHO. *J. Metamorphic Geology.* 27, 55–70. doi:10.1111/j.1525-1314.2008.00803.x

White, R. W., Powell, R., Holland, T. J. B., and Worley, B. A. (2000). The Effect of TiO_2 and Fe_2O_3 on Metapelitic Assemblages at Greenschist and Amphibolite Facies Conditions: Mineral Equilibria Calculations in the System K_2O-FeO-MgO-Al_2O_3 -SiO_2 -H_2O-TiO_2 -Fe_2O_3. *J. Metamorphic Geology.* 18, 497–511. doi:10.1046/j.1525-1314.2000.00269.x

White, R. W., Powell, R., Holland, T. J. B., Johnson, T. E., and Green, E. C. R. (2014). New mineral Activity-Composition Relations for Thermodynamic Calculations in Metapelitic Systems. *J. Meta. Geol.* 32, 261–286. doi:10.1111/jmg.12071

Whitney, D. L., and Davis, P. B. (2006). Why Is Lawsonite Eclogite So Rare? Metamorphism and Preservation of Lawsonite Eclogite, Sivrihisar, Turkey. *Geol* 34 (6), 473–476. doi:10.1130/g22259.1

Wilde, S. A., Zhao, G., and Sun, M. (2002). Development of the North China Craton during the Late Archaean and its Final Amalgamation at 1.8 Ga: Some Speculations on its Position within a Global Palaeoproterozoic Supercontinent. *Gondwana Res.* 5, 85–94. doi:10.1016/s1342-937x(05)70892-3

Xiao, W. J., Windley, B. F., Hao, J., and Zhai, M. G. (2003). Accretion Leading to Collision and the Permian Solonker Suture, Inner Mongolia, China: Termination of the central Asian Orogenic belt. *Tectonics* 22, 1069–1088. doi:10.1029/2002tc001484

Xu, B., Charvet, J., and Zhang, F. Q. (2001). Primary Study on Petrology and Geochronology of the Blueschist in Sunidzuoqi, Northern Inner Mongolia. *Chin. J. Geology.* 36, 424–434. (in Chinese with English abstract).

Xu, B., Charvet, J., Chen, Y., Zhao, P., and Shi, G. (2013). Middle Paleozoic Convergent Orogenic Belts in Western Inner Mongolia (China): Framework, Kinematics, Geochronology and Implications for Tectonic Evolution of the Central Asian Orogenic Belt. *Gondwana Res.* 23, 1342–1364. doi:10.1016/j.gr.2012.05.015

Xu, B., Zhao, P., Bao, Q. Z., Zhou, Y. H., Wang, Y. Y., and Luo, Z. W. (2014). Preliminary Study on the Pre-Mesozoic Tectonic Unit Division of the Xing-Meng Orogenic Belt (XMOB). *Acta Petrol. Sin.* 30, 1841–1857. (in Chinese with English abstract). doi:10.1016/j.pgeola.2014.02.004

Xu, B. W., Xi, A. H., Ge, Y. H., Liu, J., Wang, M. Z., and Fang, C. (2015). Zircon U-Pb Ages of the Late Paleozoic A-Type Granites in Chifeng, Inner Mongolia and its Tectonic Significance. *Acta Geol. Sin.* 1, 58–69. (in Chinese with English abstract). doi:10.3321/j.issn:1000-0569.2005.03.006

Xue, H. M., Guo, L. J., Hou, Z. Q., Zhou, X. W., Tong, Y., and Pan, X. F. (2009). The Xilingele Complex from the Eastern Part of the Central Asian-Mongolia Orogenic Belt, China: Products of Early Variscan Orogeny Other Than Ancient Block: Evidence from Zircon SHRIMP U–Pb Ages. *Acta Petrol. Sin.* 25, 2001–2010.

Yarmolyuk, V. V., Kovalenko, V. I., Sal'nikova, E. B., Kozakov, I. K., Kotov, A. B., Kovach, V. P., et al. (2005). U-pb Age of Syn- and Postmetamorphic Granitoids of South Mongolia: Evidence for the Presence of Grenvillides in the Central Asian Fold belt. *Doklady Earth Sci.* 404, 986–990.

Yarmolyuk, V. V., Kovalenko, V. I., Sal'nikova, E. B., Kovach, V. P., Kozlovsky, A. M., Kotov, A. B., et al. (2008). Geochronology of Igneous Rocks and Formation of the Late Paleozoic South Mongolian Active Margin of the Siberian Continent. *Stratigr. Geol. Correl.* 16, 162–181. doi:10.1134/s0869593808020056

Zhang, S.-H., Zhao, Y., Song, B., Yang, Z.-Y., Hu, J.-M., and Wu, H. (2007). Carboniferous Granitic Plutons from the Northern Margin of the North China Block: Implications for a Late Palaeozoic Active continental Margin. *J. Geol. Soc.* 164, 451–463. doi:10.1144/0016-76492005-190

Zhang, S. H., Zhao, Y., Song, B., Hu, J. M., Liu, S. W., Yang, Y. H., et al. (2009). Contrasting Late Carboniferous and Late Permian-Middle Triassic Intrusive Suites from the Northern Margin of the north China Craton. *Geol. Soc. Am. Bull.* 121, 181–200. doi:10.1130/B26157.1

Zhang, Y. P., Su, Y. Z., and Li, J. C. (2010). Regional Tectonic Significance of the Late Silurian Xibiehe Formation in central Inner Mongolia, China. *Geol. Bull. China* 29, 1599–1605. (in Chinese with English abstract). doi:10.1017/S0004972710001772

Zhang, J. R., Chu, H., Wei, C. J., and Wang, K. (2014). Geochemical Characteristics and Tectonic Significance of Meta-Basic Volcanics in the Ondor Sum Group, Central Inner Mongolia. *Acta Petro. Sin.* 30, 1935–1947.

Zhang, J., Wei, C., Chu, H., and Chen, Y. (2016). Mesozoic Metamorphism and its Tectonic Implication along the Solonker Suture Zone in central Inner mongolia, china. *Lithos* 261, 262–277. doi:10.1016/j.lithos.2016.03.014

Zhang, J.-R., Wei, C.-J., and Chu, H. (2018b). High-temperature and Low-pressure metamorphism in the Xilingol Complex of central Inner Mongolia, China: An Indicator of Extension in a Previous Orogeny. *J. Metamorph Geol.* 36, 393–417. doi:10.1111/jmg.12297

Zhao, G., Wilde, S. A., Cawood, P. A., Sun, M., and Lu, L. Z. (2001). Archean Blocks and Their Boundaries in the North China Craton: Lithological, Geochemical, Structural and P-T Path Constraints and Tectonic Evolution. *Precambrian Res.* 107, 45–73. doi:10.1016/s0301-9268(00)00154-6

Zhao, G., Cawood, P. A., Wilde, S. A., and Sun, M. (2002). Review of Global 2.1-1.8 Ga Orogens: Implications for a Pre-Rodinia Supercontinent. *Earth-Sci. Rev.* 59, 125–162. doi:10.1016/s0012-8252(02)00073-9

Zhicheng Zhang, Z., Li, K., Li, J., Tang, W., Chen, Y., and Luo, Z. (2015). Geochronology and Geochemistry of the Eastern Erenhot Ophiolitic Complex: Implications for the Tectonic Evolution of the Inner Mongolia-Daxinganling Orogenic Belt. *J. Asian Earth Sci.* 97, 279–293. doi:10.1016/j.jseaes.2014.06.008

Zhou, J.-B., and Wilde, S. A. (2013). The Crustal Accretion History and Tectonic Evolution of the NE China Segment of the Central Asian Orogenic Belt. *Gondwana Res.* 23, 1365–1377. doi:10.1016/j.gr.2012.05.012

Zhou, J. B., Wang, B., Zeng, W. S., and Cao, J. L. (2014). Detrital Zircon U-Pb Dating of the Zhalantun Metamorphic Complex and its Tectonic Implications, Great Xing'an, NE China. *Acta Petrol. Sin.* 30, 1879–1888.

Conflicts of Interest: The authors declare that the research was conducted in the absence of any commercial or financial relationships that could be construed as a potential conflict of interest.

Publisher's Note: All claims expressed in this article are solely those of the authors and do not necessarily represent those of their affiliated organizations, or those of the publisher, the editors and the reviewers. Any product that may be evaluated in this article, or claim that may be made by its manufacturer, is not guaranteed or endorsed by the publisher.